

1 **The effect of more realistic forcings and boundary**
2 **conditions on the modelled geometry and sensitivity**
3 **of the Greenland ice-sheet Investigating the**
4 **sensitivity of numerical model simulations of the**
5 **modern and future response of the Greenland ice-**
6 **sheet to climate change**

7
8 **E.J. Stone¹, D.J. Lunt¹, I.C. Rutt², E. Hanna³**

9 [1] {BRIDGE, School of Geographical Sciences, University of Bristol, UK}

10 [2] {School of the Environment and Society, Swansea University, UK}

11 [3] {Department of Geography, University of Sheffield, Sheffield, UK}

12 Correspondence to: E. J. Stone (emma.j.stone@bristol.ac.uk)

13
14 **Abstract**

15 Ice thickness and bedrock topography are essential boundary conditions for numerical
16 modelling of the evolution of the Greenland ice-sheet (GrIS). The datasets currently in
17 use by the majority of GrIS modelling studies are over two decades old and based on
18 data collected from the 1970s and 80s. We use a newer, high-resolution Digital
19 Elevation Model of the GrIS and new temperature and precipitation forcings to drive
20 the Glimmer ice-sheet model offline under steady state, present day climatic
21 conditions. Comparisons are made ~~in terms~~ of ice-sheet geometry between these new
22 datasets and older ones used in the EISMINT-3 exercise. We find that changing to the
23 newer bedrock and ice thickness makes the greatest difference to Greenland ice
24 volume and ice surface extent. When all boundary conditions and forcings are
25 simultaneously changed to the newer datasets the ice-sheet is ~~3325~~³³²⁵% larger in volume
26 compared with observation and ~~174~~¹⁷⁴% larger than that modelled by EISMINT-3.

27
28 We performed a tuning exercise to improve the modelled present day ice-sheet.
29 Several solutions were chosen in order to represent improvement in different aspects
30 of the GrIS geometry: ice thickness, ice volume and ice surface extent. We applied
31 these new ~~parameter sets for setups of~~ Glimmer to several future climate scenarios

1 where atmospheric CO₂ concentration was elevated to 400, 560 and 1120 ppmv
2 (compared with 280 ppmv in the control) using a fully coupled General Circulation
3 Model. Collapse of the ice-sheet was found to occur between 400 and 560 ppmv, a
4 threshold substantially lower than previously modelled using the standard EISMINT-3
5 setup. This work highlights the need to assess carefully boundary conditions and
6 forcings required by ice-sheet models, particularly in terms of the abstractions
7 required for large scale ice-sheet models, and the implications that these can have on
8 predictions of ice-sheet geometry under past and future climate scenarios.

9

10 1 Introduction

11 Complete melting of the Greenland ice-sheet (GrIS) would raise sea level by as much
12 as 7.3 m (Bamber et al., 2001), and could be associated with other major climatic
13 effects such as changes in the thermohaline circulation and oceanic heat transport due
14 to enhanced freshwater fluxes (Fichefet et al., 2003). Estimates of the GrIS's
15 contribution to sea level change during the period 1993 to 2003 range between +0.14
16 to +0.28 mm yr⁻¹ (IPCC, 2007), although recent estimates suggest as much as +0.75
17 mm yr⁻¹ for 2006-2009 (van den Broeke et al., 2009; Velicogna, 2009) linked with
18 significant recent increases in GrIS melt, runoff and mass loss (Hanna et al., 2008;
19 Rignot et al., 2008). Recent model projections suggest that the GrIS could be
20 eliminated within a few millennia for global warming between 1.9 to 4.6°C relative to
21 pre-industrial temperatures (Gregory and Huybrechts, 2006). These projections are
22 based on a numerical model which does not include a representation of fast-flowing
23 outlet glaciers. These glaciers have been observed to undergo dynamic changes in
24 recent years, resulting in faster ice flow and consequent ice loss (Howat et al., 2007;
25 Joughin et al., 2004; Luckman et al., 2006; Rignot et al., 2008; Rignot and
26 Kanagaratnam, 2006), meaning that the model probably underestimates the rate of
27 mass-loss from the GrIS.

28

29 The majority of recent modelling studies of the GrIS use the data assembled for the
30 EISMINT (European Ice-sheet Modelling INiTiative) model intercomparison project
31 as a present day representation of the GrIS. Because the description of the data is
32 included in the report from the 3rd EISMINT workshop (Huybrechts, 1997), we refer
33 to them here as the EISMINT-3 data. The data consist of a Digital Elevation Model

1 (DEM) of ice thickness and bedrock elevation, and parameterised temperature and
2 precipitation fields, onto which climate anomalies are typically superimposed (e.g.
3 Driesschaert et al., 2007; Greve, 2000; Huybrechts and de Wolde, 1999; Ridley et al.,
4 2005; Lunt et al., 2008; Lunt et al., 2009) . The high-resolution bedrock and ice
5 thickness used in EISMINT-3 are nearly two decades old and are based on data
6 collated during the 1970s and 1980s. More recent and accurate datasets for the
7 boundary conditions of bedrock topography and ice thickness ([Bamber et al., 2001](#)) as
8 well as temperature ([Hanna et al., 2005; Hanna et al., 2008](#)) and precipitation
9 ([ECMWF, 2006](#)) forcings are now available ([Bamber et al., 2001; ECMWF, 2006;](#)
10 [Hanna et al., 2005; Hanna et al., 2008](#)). Differences in these datasets could have
11 considerable impacts on the modelled evolution of the GrIS and hence the resulting
12 ice-sheet volume and geometry, for simulations of past, modern and future climates.
13

14 In this paper, we use the Glimmer ice-sheet model (Rutt et al., 2009) to investigate
15 and compare the impact on the modelled steady-state ice-sheet of two sets of
16 boundary conditions: those used in the EISMINT-3 exercise, and the more recent and
17 up-to-date datasets. Furthermore, we perform a tuning exercise with respect to the
18 most recent datasets in order to determine the values of various ice-sheet model
19 parameters which give the best fit between modelled and observed geometry for
20 present day conditions. Finally, we use the results from the tuning exercise to assess
21 the impact of different parameter combinations on future warming scenarios with
22 atmospheric CO₂ held at 400 ppmv, 560 ppmv and 1120 ppmv (compared with 280
23 ppmv in the control) where the ice-sheet model is driven offline using output from a
24 fully-coupled General Circulation Model (GCM). Most recent sensitivity studies have
25 only used one set of ice-sheet model parameters (e.g. ablation coefficients) for
26 simulations of future ice-sheet evolution (e.g. Alley et al., 2005 Driesschaert et al.,
27 2007; Mikolajewicz et al., 2007; Ridley et al., 2005). Our results highlight the need to
28 use a range of ice model parameter sets in order to assess their impact on future ice-
29 sheet climate scenarios.
30

31 **2 Model description**

32 We use the 3D thermomechanical ice-sheet model Glimmer version 1.0.4 (Rutt et al.,
33 2009). Although not the most recent version of the model, we use this version for

1 consistency with our previous work (e.g. Lunt et al, 2008, 2009). The core of the
2 model is based on the ice-sheet model described by Payne (1999). All physical
3 constants and parameters discussed in this section are given in Table 1. Here we
4 describe the parts of the model which pertain to the model parameters which we tune
5 in the subsequent sections. A full description of the model can be found in Rutt et al.
6 (2009).

7

8 The ice thickness (H) evolution is driven by the mass conservation equation

9

10
$$\frac{\partial H}{\partial t} = -\nabla \cdot (\bar{\mathbf{u}} H) + B - S, \quad (1)$$

11

12 where \mathbf{u} is the horizontal velocity and $\bar{\mathbf{u}}$ is the horizontal velocity averaged over the
13 ice thickness, B is the surface mass balance rate and S is the basal melt rate. Equation
14 (1) is solved using a linearised semi-implicit method.

15

16 The ice dynamics are represented with the widely-used shallow-ice approximation,
17 which assumes ice deformation occurs as shear strain only, so that

18

19
$$\mathbf{u}(z) = \mathbf{u}(b) - 2(\rho_i g)^n |\nabla s|^{n-1} \nabla s \int_b^z A(T^*) (s - z')^n dz', \quad (2)$$

20

21 where s is the ice-sheet surface altitude, b is the bedrock altitude, g is the acceleration
22 due to gravity, ρ_i is the ice **sheet** density, x and y the horizontal coordinates and z the
23 vertical coordinate, positive upward. $A(T^*)$ is an empirical parameter where T^* is the
24 absolute temperature corrected for the dependence of the melting point on pressure.

25

26 Equation (2) implicitly uses the non-linear viscous flow law (Glen's flow law) to
27 relate deformation rate and stress. The two parameters are the exponent, n , and the
28 ice flow law parameter, $A(T^*)$, which follows the Arrhenius relationship

29

30
$$A(T^*) = fa \exp\left(-\frac{Q}{RT^*}\right), \quad (3)$$

31

1 where a is a temperature-independent material constant, Q is the activation energy and
2 R is the universal gas constant. In Eq. (3), f is the flow enhancement factor, a tuneable
3 factor which can be used to change the flow law parameter, and, hence, change the ice
4 flow velocity. The flow enhancement factor-speed of ice flow, and which accounts
5 for ice impurities and development of anisotropic ice fabrics, effects not represented
6 by separate parameters in the model.

7

8 The model is formulated on a Cartesian x - y grid, and takes as input the surface mass-
9 balance and mean air temperature at each time step. In the present work, the ice
10 dynamics time step is one year. To simulate the surface mass-balance, we use the
11 Positive Degree Day (PDD) scheme described by Reeh (1991). The basis of the PDD
12 method is the assumption that the melt, m , that takes place at the surface of the ice-
13 sheet is proportional to the time-integrated temperature above freezing point, known
14 as the positive degree day:
15

$$16 \quad m = \alpha \int_{\text{year}} \max(T(t), 0) dt, \quad (4)$$

17

18 where $T(t)$ is the near-surface air temperature and α is the PDD factor. Two PDD
19 factors which describe the rate of melting are used, one each for snow (α_s) and ice
20 (α_i), to take account of the different albedos and densityies of these materials. The
21 integral in Eq. (4) is calculated on the assumption of a sinusoidal annual variation in
22 temperature, and takes as input the mean annual temperature and half-range. Diurnal
23 and other variability is taken into account using a stochastic approach. This variability
24 is assumed to have a normal distribution with a standard deviation of 5°C. The use of
25 PDD mass-balance models is well-established in coupled atmosphere-ice-sheet
26 modelling studies of both paleoclimate (e.g. DeConto & Pollard, 2003; Lunt et al.,
27 2008) and future climate (e.g. Ridley et al., 2005, Mikolajewicz et al., 2007). All
28 precipitation is assumed to be potentially available for accumulation within the
29 Glimmer annual PDD scheme. The following possibilities are taken into account
30 when considering the total annual ablation. Melting snow is allowed to refreeze to
31 become superimposed ice up to a fraction, w , of the original snow depth. When the
32 ability of the snow to hold meltwater is exceeded but the potential snow ablation is
33 less than the total amount of precipitation (amount of snow available), run-off can

1 occur. If the potential snow ablation is greater than precipitation, snow will melt first,
2 and then ice, such that the total ablation is equivalent to the sum of snow melt (total
3 precipitation minus the amount of meltwater held in refreezing) and the sum of ice
4 melt (calculated by deducting from the total number of degree days from the number
5 of degree days need to melt all snow fall and converted to ice melt). Therefore, the
6 net annual mass balance is the difference between the total annual precipitation and
7 the total annual ablation.

8

9 Glimmer also includes a representation of the isostatic response of the lithosphere,
10 which is assumed to behave elastically, based on the model of Lambeck and
11 Nakiboglu (1980). The timescale for this response is 3,000 years. In all model runs
12 described below, the isostasy model is initialised on the assumption that the present
13 day bedrock depression is in equilibrium with the ice-sheet load. Although this
14 assumption may not be entirely valid, any rates of change will not have a significant
15 influence for present day geometry (Huybrechts and de Wolde, 1999).

16

17 Geothermal heat flux (G) can be supplied to the model as a constant or a spatially
18 varying field (both of which are explored in Sec. 5.2), and a thermal bedrock model
19 (Ritz, 1987) takes the thermal evolution of the uppermost bedrock layer into account
20 where initial conditions for the temperature field are found by applying the
21 geothermal heat flux to an initial surface temperature.

22

23 The forcing data (temperature and precipitation) are transformed onto the ice model
24 grid using bilinear interpolation. In the case of the near-surface air temperature field
25 (T_a), a vertical lapse-rate correction is used to take account of the difference between
26 the high-resolution (20 km in this case) surface topography seen within Glimmer (s_G),
27 and that represented by the forcing data (s) (in this case a latitude longitude grid 1°
28 by 1° grid or approximately 111 km resolution), such that

29

$$30 T_a' = T_a + L_G (s_G - s). \quad (5)$$

31

32 Here, T_a' is the lapse corrected surface temperature as seen by the high-resolution ice-
33 sheet model and, L_G is the vertical atmospheric lapse rate and s_G is the low resolution

1 | ~~of the climate model~~. The use of a lapse-rate correction to better represent the local
2 | temperature is established in previous work (e.g. Glover, 1999; Hanna et al., 2005;
3 | Hanna et al., 2008; Pollard and Thompson, 1997).

4

5 | **3 The datasets**

6 | **3.1 EISMINT-3 intercomparison experimental design**

7 | In order to evaluate the consistency in predictions between different ice-sheet models,
8 | the EISMINT validation exercise was set up (Huybrechts and Payne, 1996).
9 | EISMINT-3 (Huybrechts, 1997) was the final ~~part~~~~section~~ of this exercise which
10 | involved ~~realistically~~ modelling changes in ice mass given a climate scenario for a
11 | number of different ice-sheet models with prescribed parameters and climate forcings
12 | (Van der Veen and Payne, 2004). This included the evolution of GrIS mass changes
13 | under a) steady-state present climate conditions, b) a transient climate such as the
14 | last climatic cycle based on GRIP ice core data and c) ~~finally~~ future greenhouse
15 | warming. By modelling present day steady-state conditions, it is possible to test the
16 | validity of the reconstructions that the models produce, by comparing the model
17 | predictions with observations of the present day ice-sheet. In the EISMINT-3
18 | standard, the initial condition of bedrock and surface elevation was compiled by
19 | Letreguilly et al. (1991) on a 20~~-~~km Cartesian grid. The precipitation forcing is from
20 | Ohmura and Reeh (1991) and the temperature forcing is given by the following
21 | parameterisations (Huybrechts and de Wolde, 1999; Ritz et al. 1997) which were
22 | themselves based on observed surface temperature data (Ohmura, 1987)

23

24 | $T_{ann} = 49.13 - L_a H_{surf} - 0.7576\Phi$, (6)

25 | $T_s = 30.78 - L_s H_{surf} - 0.3262\Phi$, (7)

26

27 | where H_{surf} is the surface elevation (m), Φ is the geographical latitude (in degrees and
28 | positive), T_{ann} is the mean annual temperature, T_s is the summer temperature (both in
29 | °C), and $L_a = -7.992$, $L_s = -6.277$ are annual and summer atmospheric lapse rates
30 | respectively (in °C km⁻¹).

31

1 **3.2 Recent boundary conditions/forcings**

2 New and more accurate bedrock and surface elevation datasets are now available with
3 significant differences in ice volume (~4% increase) and ice thickness (factor of 10)
4 around the margins compared with the Letreguilly dataset (Bamber et al., 2001). This
5 new dataset utilises improvements in the boundary conditions of surface elevation. Ice
6 thicknesses were derived from combining data collected in the 1970s with new data
7 obtained from an ice penetrating radar system from 1993 to 1999. The surface
8 bedrock topography was subsequently derived from a DEM of the ice-sheet and
9 surrounding rocky outcrops. The DEM is produced from a combination of satellite
10 remote sensing and cartographic datasets. In contrast, the Letreguilly dataset is based
11 on cartographic maps for ice free regions and radio echoing sounding for
12 determination of ice thickness. No satellite-derived products were used. The Bamber
13 dataset has the advantage of significantly more sources of accurate data and better
14 coverage. The Bamber dataset is on a 5_-km resolution grid; for the purposes of the
15 present work, it was interpolated onto a 20_-km resolution grid, generated by
16 pointwise averaging on the same projection. Henceforth, we will refer to the
17 EISMINT-3 bedrock and ice thickness dataset as the ‘Letreguilly’ dataset and the
18 more recent dataset as the ‘Bamber’ dataset.

19
20 The precipitation data used in EISMINT-3 (Ohmura and Reeh, 1991) is based purely
21 on precipitation measurements from meteorological stations (35) and pits and cores in
22 the interior of the ice-sheet. Not only is this based on a small number of data
23 locations but the accuracy of measurements is also a matter of contention. Catch
24 efficiency, particularly for solid precipitation, by gauges is somewhat reduced by
25 turbulent winds along with the potential for snow to be blown out of gauges (Yang,
26 1999). Measurement error may reach 100% during the winter months, when
27 accumulation is most important for mass balance (Serreze et al., 2005). We make use
28 of precipitation data derived from ERA-40 reanalysis from 1979-2001 (ECMWF,
29 2006) on a regular latitude-longitude 1° by 1° resolution grid. ERA-40 reanalysis is
30 produced using a data assimilation technique which consists of a number of analysis
31 steps (Uppala et al., 2005). Background information is produced from a short-range
32 forecast and combined with observations for this same period of the forecast to
33 produce an ‘analysis’. Statistically-based estimates of errors are used for the synthesis

1 of background forecast and observation. Each forecast is initialised from the most
2 recent previous analysis step. Observations do not consist of all meteorological
3 variables but the analysis is complete in terms of the variables chosen. As such,
4 variables can be produced from analysis (e.g. temperature) while others are purely
5 based on forecast and are, therefore, not constrained by observations. (Uppala et al.,
6 2005). In ERA-40, precipitation is one such variable produced by the forecast rather
7 than by the analysis in the ECMWF model. However, it has been shown to be
8 reasonable for Greenland (Serreze et al., 2005). Validation against Danish
9 Meteorological Institute (DMI) coastal stations results in a 36% mean excess for
10 ERA-40 (Hanna and Valdes, 2001), although the inaccuracies in gauge measurements
11 mean that this should be treated with some caution. In terms of other reanalysis
12 products available, comparison studies have shown ERA-40 to be superior to
13 NCEP/NCAR datasets in terms of smaller biases, ability to capture large scale
14 patterns of precipitation and its depiction of interannual variability, deeming ERA-40
15 a more suitable choice (Bromwich et al., 1998; Hanna et al., 2006; Serreze et al.,
16 2005; Serreze and Hurst, 2000).

17

18 The near-surface air temperature forcing used in the EISMINT-3 exercise is based on
19 a parameterisation of surface temperature compiled by Ohmura (1987), which has a
20 latitudinal and altitude dependency (see Eq. (6) and Eq. (7)). Two lapse rate values
21 are used: the mean annual lapse rate and a summer lapse rate. Currently, lapse rate in
22 Glimmer is not temporally or regionally varying so the summer lapse rate is used
23 since this is when the ablation process is strongest. The parameterisations were
24 constructed to fit data from 49 meteorological stations. ~~A new parameterisation based~~
25 ~~on more up-to-date Automatic Weather Station data is now available with a similar~~
26 ~~form to Eq. (6) and Eq. (7) (Fausto et al., 2009). However, we have chosen the novel~~
27 ~~approach to use the original temperature observations rather than a highly tuned~~
28 ~~parameterisation. Several datasets exist in terms of satellite and re-analysis products.~~
29 ~~For satellite datasets, temperature data are available from the Advanced Very High~~
30 ~~Resolution Radiometer (AVHRR) Polar Pathfinder (APP) from 1982–2004 which is~~
31 ~~collated twice a day at the local solar times of 1400 and 0400. Although the data is~~
32 ~~initially on a 5 km resolution it is sub-sampled at 25 km pixels. The APP-x product~~
33 ~~includes all-sky surface temperature with the cloudy sky surface temperatures~~
34 ~~calculated using an empirical relationship between clear-sky surface temperature,~~

1 wind speed, and solar zenith angle (daytime). However, this only applies to surface
2 temperatures over sea ice and not land. Therefore, temperatures over Greenland are
3 based only on data from clear sky retrieval with temperatures in cloudy regions
4 interpolated from clear sky areas. Although useful for comparing with present day
5 surface temperatures from climate models, this dataset is not suitable to directly force
6 an ice sheet model over Greenland. Firstly, the largest uncertainties are likely to be
7 over Greenland (Key, pers. comm.). Secondly, no associated orography exists which
8 is used to downscale from the resolution of the forcing data onto the high resolution
9 of the ice sheet model. Thirdly, sensitivity studies using Glimmer indicate that the
10 APP x temperatures were significantly too cold, in observed ice free regions such as
11 western Greenland, (by up to 12°C in western Greenland compared with EISMINT 3
12 temperatures which have at least been derived from surface observation) to reproduce
13 a reasonable modern day ice sheet without tuning ice sheet model parameters beyond
14 uncertainty ranges. This could, in part, be due to the satellite recording ice surface
15 temperatures rather than air temperature. Furthermore, clear sky retrievals errors are
16 predominantly due to uncertainties in cloud detection (Key et al., 1997) particularly
17 during the night. The low temperatures, bright surface and high elevation make
18 remote sensing over Greenland particularly difficult in terms of accurate cloud
19 detection. Instead, we use, to be consistent with precipitation, surface (2-m) air
20 temperature data derived from ERA-40 ‘corrected’ 2-m near-surface air temperatures
21 (Hanna et al., 2005). The temperatures were corrected based on their derived surface
22 lapse rates and differences between the ECMWF orography and a DEM derived from
23 the Ekholm (1996) grid (Hanna et al., 2005). Reasonable agreement exists between
24 these model-derived temperatures and observations at the DMI station locations and
25 GC-Net stations (Hanna et al., 2005). We use bilinear interpolation to transform the
26 high-resolution dataset from its Cartesian 5-km resolution grid onto a 1° by 1°
27 latitude longitude grid. Since, the dataset only covers the regions where there is ice,
28 the temperature parameterisation used in EISMINT-3 temperature is used in the ice-
29 free regions of Greenland in conjunction with the Ekholm orography. This means that
30 the sensitivity to temperature is specifically a sensitivity to the surface temperature of
31 the ice-sheet and not the ice-free regions.

32

1 **4 Sensitivity to boundary conditions and forcings**

2 In order to test the sensitivity of the ice-sheet model to the various forcing inputs and
3 boundary conditions, we performed a set of steady-state experiments [shown in Table](#)
4 [2](#), initialised from present day geometry of the ice-sheet. The model is run for 50,000
5 years in order to reach equilibrium. The configuration of the ice-sheet model is kept
6 at that of EISMINT-3 with standard parameter values as shown in Table 1. For each
7 simulation in the set, one forcing/boundary condition is changed to the most recent
8 dataset, keeping all others at that used in EISMINT-3. An additional experiment is
9 performed where all the forcings and boundary conditions are changed to the most
10 recent. Figure 1 shows the evolution of ice area extent and ice volume with time for
11 EISMINT-3 and the four sensitivity experiments.

12

13 **4.1 Bedrock and ice thickness**

14 [The quality of the bedrock topography is important in ice-sheet models since it largely](#)
15 [determines the ice thickness at regional scales. This is because topography influences](#)
16 [where the build up of snow and ice can occur and therefore is a major control on the](#)
17 [threshold of ice-sheet initiation. Furthermore, topography influences the convergence](#)
18 [and divergence of ice flow such that flow into lowland basins and valleys from](#)
19 [surrounding higher relief regions will result in faster build up of ice compared with](#)
20 [flow from an isolated upland region into a lower basin \(Payne and Sugden, 1990\). As](#)
21 [a result, the topography influences the stress, velocity and thermal regimes of the ice-](#)
22 [sheet \(Van der Veen and Payne, 2004\).](#)

23

24 [At the outset there are differences in ice thickness and bedrock topography between](#)
25 [the two bedrock and ice-thickness datasets \(see Fig. 2a and 2b\). The bedrock](#)
26 [topography around the margins is consistently higher for the Bamber dataset](#)
27 [compared with the Letreguilly dataset, with the ice thickness difference up to a factor](#)
28 [of ten to twenty thicker. When simulated to steady-state, the Bamber bedrock and ice](#)
29 [thickness datasets results in significantly \(13.7%\) greater ice volume and 11.5% larger](#)
30 [ice surface extent compared with the Letreguilly dataset. Ice extends further to the](#)
31 [northern and western margins of Greenland with a higher central dome. The initial](#)
32 [higher elevation of the ice-free bedrock of the Bamber dataset provides favourable](#)

1 conditions for ice growth where temperatures are cold enough for mass balance to
2 become positive. In these regions ice velocities are low compared with other
3 marginal regions, allowing the ice-sheet to build-up with minimal ice loss. The basal
4 temperatures are also colder than when the Letreguilly dataset is used, resulting in
5 marginally lower velocities for ice flow. This arises because the ice in the Bamber
6 dataset is thicker at the beginning of the simulation. The increase in ice volume and
7 surface extent, however, can be attributed predominately to a stronger ice-elevation
8 feedback mechanism for the Bamber dataset.

9 **4.14.2 Precipitation**

10 Changing the precipitation forcing, from that of Ohmura and Reeh (as in EISMINT-3)
11 to ERA-40, results in an increase in equilibrium ice-sheet surface extent of 2.1%.

12 However, there is almost no effect on the ice-sheet volume. This can be explained by
13 the fact- aAll precipitation that falls is assumed to fall as snow in the annual PDD
14 scheme. Since the temperature forcing has no effect on the amount of snow, it is the
15 quantity and distribution of precipitation that results in the difference in ice surface
16 extent. Figure 32 shows that the annual precipitation is up to two times greater on the
17 eastern and western margins of Greenland for ERA-40 compared with Ohmura and
18 Reeh (1991). The accumulation rate is greatest in south-east Greenland for both
19 precipitation datasets but extending further north along the eastern margin for ERA-
20 40. The extra precipitation falling over the western and eastern margins coupled with
21 a positive ice-elevation feedback results in growth and extension of the ice-sheet into
22 previously ice-free regions. However, the precipitation falling over central and north
23 Greenland is three times less for ERA-40, resulting in less accumulation in the interior
24 and lower maximum altitude of the ice sheet. These opposing effects result in similar
25 ice-sheet volumes. However, Hanna et al. (2006) show that ERA-40 is ~50% too
26 “dry” in the central northern parts of Greenland, as validated using ice-core data.
27 Furthermore, it seems increasingly likely that both the Ohmura & Reeh (1991) and
28 ERA-40 precipitation datasets underestimate precipitation and accumulation in south-
29 east Greenland, where recent regional climate model results suggest much higher than
30 previously observed precipitation rates (Burgess et al., 2009; Ettema et al., 2009;
31 Burgess et al., 2010).

32

1 **4.24.3 Temperature**

2 Changing the temperature forcing to the modified Hanna dataset results in a similar
3 almost identical ice volume (1.6% larger) compared with EISMINT-3 and an almost
4 identical reduction in the ice-sheet extent-of 2.0%. Figure 43 and Figure 54 show the
5 temperature distribution and the surface mass balance respectively at the beginning
6 and end of the experiments for EISMINT-3 temperature and the Hanna modified
7 temperature datasets. As expected, at the beginning of the simulation temperatures
8 around the margins of the GrIS are similar (same datasets) but the Hanna ERA-40
9 corrected temperatures over the ice-sheet are several degrees colder (Fig. 43a,b) . By
10 the end of the simulations, temperatures over much of Greenland have become lower
11 as a result of the positive ice-elevation feedback (Fig. 43c,d) resulting in an increase
12 in positive net mass balance in southern Greenland (see Fig. 54c,d). However, the
13 regions around the margins remain ice-free as a result of continued ablation with a net
14 negative mass balance. The model is particularly sensitive to the temperature forcing
15 around the margins of the ice-sheet, where temperatures are at zero or above and so
16 close to ablation as opposed to those in the interior where the primary mass-balance
17 change is from accumulation (Hanna et al. 2005). It is, therefore, important that
18 marginal temperatures close to where the net mass balance becomes negative are
19 resolved accurately in order to model the ablation process and the resulting geometry
20 of the GrIS.

21

22 **4.3 Bedrock and ice thickness**

23 The quality of the bedrock topography is important in ice sheet models since it largely
24 determines the ice thickness at regional scales and hence the stress, velocity and
25 thermal regimes of the ice sheet (Van der Veen and Payne, 2004). At the outset there
26 are differences in ice thickness and bedrock topography between the two bedrock and
27 ice thickness datasets (see Fig. 5a and 5b). The bedrock topography around the
28 margins is consistently higher for the Bamber dataset compared with Letreguilly with
29 ice thickness difference up to a factor of ten to twenty thicker. When simulated to
30 steady state, the Bamber bedrock and ice thickness datasets results in significantly
31 (13.7%) greater ice volume and 11.5% larger ice surface extent compared with
32 Letreguilly. Ice extends further to the northern and western margins of Greenland

1 with a higher central dome. The initial higher elevation of the ice free bedrock of the
2 Bamber dataset provides favourable conditions for ice growth where temperatures are
3 cold enough for mass balance to become positive. In these regions ice velocities are
4 low compared with other marginal regions, allowing the ice sheet to build up with
5 minimal ice loss. The basal temperatures are also colder than Letreguilly, resulting in
6 marginally lower velocities for ice flow. This arises because the ice in the Bamber
7 dataset is thicker at the beginning of the simulation. The increase in ice volume and
8 surface extent, however, can be attributed predominately to a stronger ice elevation
9 feedback mechanism for the Bamber grid.

10
11 Table 32 summarises the results of changing bedrock and ice thickness, precipitation
12 and, temperature and bedrock and ice thickness independently from EISMINT-3 to
13 the newer datasets. Bedrock and ice thickness result in the largest ice volume and ice
14 surface extent change while changing precipitation and temperature have the least
15 significantly smaller effect on the ice volume. Precipitation change acts to increase
16 the ice surface extent by a similar amount to temperature which in contrast acts to
17 reduce the ice surface extent.

18
19 Updating all the boundary conditions and forcings together results in a modelled GrIS
20 ice volume 3325% larger than observed (Bamber et al., 2001) and 164% larger than
21 EISMINT-3. The system shows some non-linearity is effectively linear since adding
22 together the difference between the EISMINT-3 case and the individual response of
23 the ice-sheet to each forcing/boundary condition results in a modelled GrIS larger
24 very similar to than when all forcings/boundary condition are varied together (see Fig.
25 1). This is the case for ice volume (1.72% smallerlarger) and ice surface extent
26 (03.16% smallerlarger). In fact, adding the forcings together in this way results in an
27 evolution in ice volume almost identical to the case when bedrock is varied
28 individually. This suggests that when the bedrock topography is varied, the ice model
29 also becomes sensitive to how this interacts with different climate forcings.

30
31 These results show that when using alternative boundary conditions and forcings
32 Glimmer gives a poorer representation of the modern ice-sheet compared with
33 observation. It is likely that some of the internal ice-sheet model parameters were
34 tuned to work with the boundary conditions used in EISMINT-3. In order to produce

1 a reasonable best fit between modelled and observed geometry we tune a number of
2 ice model parameters to work with the new datasets.

3 **5 Tuning**

4 **5.1 Tuning methodology**

5 Several parameters in large-scale ice-sheet modelling are still poorly constrained,
6 resulting in highly variable ice-sheet volume and extent depending on the values
7 prescribed in the model (Ritz et al., 1997). This necessitates the tuning of the ice-sheet
8 model with the recent datasets in order to determine the optimal ice-sheet for steady-
9 state conditions (i.e. closest geometry to reality). Previous work (e.g. Ritz et al.,
10 1997) has looked at the sensitivity of ice-sheet volume and extent to a number of
11 parameters, including flow enhancement factor (f) in the flow law (see Eq. 3), the
12 sliding coefficient, the geothermal heat flux (G) and the coefficients (PDD factors) of
13 the ablation parameterisation for ice (α_i) and snow (α_s) (see Eq. 4). In addition,
14 Hebeler et al. (2008a) also looked at the effect on ice volume and extent of the
15 Fennoscandian ice-sheet during the Last Glacial Maximum from uncertainty in model
16 parameters (e.g. lapse rate in addition to those mentioned above) and climate forcing
17 by performing a parametric uncertainty analysis using Glimmer, and found a variation
18 of 65% in equilibrium ice sheet extent due to uncertainty in the parameters used in the
19 ice sheet model and up to 6.6% due to uncertainty in topographic input.

20
21 The most common methodology in glaciological modelling sensitivity studies is to
22 vary one parameter at a time within a prescribed range while holding all others
23 constant (e.g. Van de Wal and Oerlemans, 1994 Essery and Etchevers, 2004; Fabre et
24 al., 1995; Huybrechts and de Wolde, 1999; Pattyn, 2003; Ritz et al., 1997). We build
25 on the methodology used in this previous work by using the statistical method of
26 Latin-Hypercube Sampling (LHS) (an efficient variant of the Monte Carlo approach)
27 which generates a distribution of plausible parameter sets within a prescribed set of
28 ranges (McKay et al., 1979). It uses a stratified-random procedure where values are
29 sampled from the prescribed distribution of each variable. The cumulative
30 distribution of each variable is divided into N equiprobable intervals and a value
31 selected randomly from each interval. The N values obtained for each variable are
32 paired randomly with the other variables. The method assumes that the variables are

1 independent of one another (which is the case here) and ensures a full coverage of the
2 range of each variable. LHS has been used in a number of applied scientific
3 disciplines including analysing uncertainty in vegetation dynamics (Wramneby et al.,
4 2008), rainfall models for climate assessment (Murphy et al., 2006) and climate/ocean
5 models (Edwards and Marsh, 2005; Schneider von Deimling et al., 2006). However,
6 it has yet to be used in large-scale ice-sheet modelling. The advantage of this
7 methodology is that it is an efficient method to test the response of the ice-sheet to
8 many different combinations of parameters by ensuring sufficient coverage of the
9 parameter space without having to test all possible model combinations (which would
10 be extremely computationally expensive). In this way, by varying more than one
11 parameter at a time (as for any multivariate sampling method) it also allows the
12 influence of each parameter on the outcome of the model simulations to be assessed
13 while taking interactions with other parameters into account.

14

15 We investigate not only the result of uncertainty in the following parameters, but also
16 which combination gives the optimal fit to the present day GrIS. The geometry of the
17 GrIS is controlled by the flow of ice from the ice divide in the interior towards the
18 coastal regions due to internal deformation where at relatively low altitudes, typically
19 ~ 2000 m, ice mass is lost by melting according to the PDD scheme. Ice mass can
20 also be lost by basal melt and/or the process of basal sliding which can increase the
21 flow of ice to regions of ablation at the edge of the ice-sheet. Since basal sliding is
22 not included in these simulations, this process will not be considered but the likely
23 impact of this missing process is highlighted in the discussion section. We choose the
24 following parameters to tune since they fundamentally affect the processes described
25 in Sect. 2. Firstly, the flow rate of ice can be tuned with the flow enhancement factor,
26 f (see Eq. 3), to simulate ice flow reasonably accurately. Secondly, the surface mass
27 balance can be tuned using the PDD factors and vertical lapse rate. The melting of ice
28 at low altitudes is determined by ablation, which in this study is calculated according
29 to the annual PDD scheme. Since this uses an empirical relationship, we choose to
30 vary the PDD factors for ice (α_i) and snow (α_s) within the ranges obtained through
31 measurement studies (see below), and therefore influence the amount of melting that
32 can occur in the ablation zones. These parameters will not, however, alter the position
33 of these zones. This instead can be achieved by varying the vertical atmospheric lapse
34 rate (L_G), which can influence the regions where ablation has the potential to occur.

1 Thirdly, ice loss by basal melt without sliding can be achieved by varying the
2 geothermal heat flux (G), which can raise the basal ice layer temperature to its
3 pressure melting point.

4

5 LHS requires a maximum and minimum bound for each tuneable parameter to be
6 defined. Here we discuss the bounds we have selected for each value, shown in Table
7 | [43](#).

8

9 The range for the flow enhancement factor for this study is between 1 and 5.
10 According to Dahl-Jensen and Gundestrup (1987), borehole measurements from Dye-
11 3 give a mean enhancement factor of around 3 with a maximum value of 4.5 and a
12 minimum value of around 1 for ice deposited during the Wisconsin. This is the range
13 | used by Ritz et al. (1997) and Hebeler et al. (2008a) for their sensitivity studies.
14 Values within this range have also been used in other work (e.g. Fabre et al., 1995;
15 Greve and Hutter, 1995; Huybrechts et al., 1991; Letreguilly et al., 1991).

16

17 The global average geothermal heat flux (oceans and continents) is estimated at
18 | $87 \times 10^3 \text{ mW m}^{-2}$ (Banks, 2008). Since it is difficult to measure geothermal heat flux
19 beneath the ice directly, many studies (e.g. Calov and Hutter, 1996; Huybrechts and
20 de Wolde, 1999; Ritz et al., 1997) assume that the average value for Pre-Cambrian
21 | Shields (Greenland bedrock) is $\sim 42 \times 10^3 \text{ mW m}^{-2}$ (Lee, 1970) although a value of
22 | $50 \times 10^3 \text{ mW m}^{-2}$ is used in EISMINT-3, and values as high as $65 \times 10^3 \text{ mW m}^{-2}$ have
23 also been used (Greve, 2000). In terms of more recent measurements inferred from
24 | ice cores, the lowest recorded heat flux over Greenland is $38.7 \times 10^3 \text{ mW m}^{-2}$ from
25 Dye-3 (Dahl-Jensen and Johnsen, 1986). The average value for continents is 61×10^3
26 | mW m^{-2} (Lee, 1970). Although values as high as $140 \times 10^3 \text{ mW m}^{-2}$ have been
27 measured at NGRIP (Buchardt and Dahl-Jensen, 2007; NGRIP, 2004) and values as
28 | low as $20 \times 10^3 \text{ mW m}^{-2}$ modelled (Greve, 2005), we use the range between 38×10^3
29 | and $61 \times 10^3 \text{ mW m}^{-2}$ for the geothermal heat flux over the whole of Greenland. This is
30 similar to the ranges used by previous sensitivity studies (Greve and Hutter, 1995;
31 Ritz et al., 1997). We also investigate the effect of a spatially varying geothermal heat
32 flux over Greenland (Shapiro and Ritzwoller, 2004) with all other parameters set at
33 the default EISMINT-3 values. We compare this with the standard setup where the
34 | geothermal heat flux is $50 \times 10^3 \text{ mW m}^{-2}$ over Greenland.

1
2 Ice and snow ablation is related to air temperature by the PDD factor, which
3 represents a simplification of processes that describe the energy balance of the glacier
4 and overlying boundary layer. The implausibility of using one universal factor being
5 valid for all of Greenland presents a challenge. The standard value used for ice by
6 many modellers is $8 \text{ mm d}^{-1} \text{ }^{\circ}\text{C}^{-1}$. (e.g. Huybrechts and de Wolde, 1999, Ritz et al.
7 1997). However, Braithwaite (1995) concluded that PDD factors for ice are generally
8 larger than the standard value and could be as high as $20 \text{ mm d}^{-1} \text{ }^{\circ}\text{C}^{-1}$. The PDD
9 factor for snow has also been estimated to range between 3 and $5 \text{ mm d}^{-1} \text{ }^{\circ}\text{C}^{-1}$ with a
10 standard value of 3 used by most modelling studies (Braithwaite, 1995). Modelling of
11 PDD factors using a regional climate model in southern Greenland found ranges for
12 the ice PDD factor α_i between 8 and $40 \text{ mm d}^{-1} \text{ }^{\circ}\text{C}^{-1}$ and the snow PDD factor α_s
13 between 3 and $15 \text{ mm d}^{-1} \text{ }^{\circ}\text{C}^{-1}$ (Lefebvre et al., 2002). Other GrIS modelling studies
14 have used higher PDD factors than the standard (e.g. Greve, 2000; Vizcaino et al.,
15 2008). We use a range for the ice PDD factor α_i between $8 \text{ mm d}^{-1} \text{ }^{\circ}\text{C}^{-1}$ and 20 mm d^{-1}
16 $\text{ }^{\circ}\text{C}^{-1}$ and a range for the snow PDD factor α_s between $3 \text{ mm d}^{-1} \text{ }^{\circ}\text{C}^{-1}$ and $5 \text{ mm d}^{-1} \text{ }^{\circ}\text{C}^{-1}$
17 .
18

19 The near-surface atmospheric lapse rate varies both spatially and temporally over
20 Greenland. Lapse rate is known to vary significantly throughout the year due in part to
21 changes in moisture content of the atmosphere. Observations from automatic weather
22 stations indicate a mean annual lapse rate along the surface slope of $-7.1 \text{ }^{\circ}\text{C km}^{-1}$ with
23 seasonally varying lapse rates varying between $-4.0 \text{ }^{\circ}\text{C km}^{-1}$ (in summer) and $-10.0 \text{ }^{\circ}\text{C}$
24 km^{-1} (in winter) (Steffen and Box, 2001). Relationships derived from ERA-40
25 reanalysis data also yield less negative summer lapse rates of as low as $-4.3 \text{ }^{\circ}\text{C km}^{-1}$ at
26 the margins and a more negative annual lapse rate of $-8.2 \text{ }^{\circ}\text{C km}^{-1}$ for the bulk of the
27 GrIS (Hanna et al., 2005). Since Glimmer only uses one value for lapse rate we vary it
28 between -4 and $-8.2 \text{ }^{\circ}\text{C km}^{-1}$ which corresponds to the seasonal variation in lapse rate.
29 This also encompasses the range used in the EISMINT-3 standard experiment for
30 annual and summer lapse rate given in Eq. (6) and Eq. (7).
31

1 **5.2 Sensitivity to tuning parameters**

2 We generate 250 plausible parameter sets using LHS and run the ice-sheet model for
3 50,000 years under a steady-state present day climate. Figure 6 shows the distribution
4 of the 250 experiments with each experiment represented by a circle for three of the
5 five tuneable parameters and the other two represented by size and colour of the
6 circle.

7

8 In order to analyse the 250 experiments' ice-sheet geometries, ~~three-four~~ diagnostics
9 are chosen and analysed using two skill scores. ~~Three of t~~These diagnostics are ice
10 surface extent, total ice volume and maximum ice thickness. Their ability to replicate
11 observation is described by the absolute error skill score, where zero is a perfect
12 match. In addition, the Normalised Root Mean Square Error (NRMSE) skill score
13 ~~for in~~ ice thickness is used to measure the spatial fit of ice thickness over the model
14 domain. Again, zero would describe a perfect match between modelled ice
15 thicknesses and observed. We calculate the diagnostics with respect to the DEM
16 derived by Bamber et al. (2001), interpolated to 20~~-~~km resolution. Figure 7
17 summarises the sensitivity of maximum ice thickness error, ice surface extent and ice
18 volume error to the five tuneable parameters.

19

20 Maximum ice thickness and ice volume are dependent on the flow law enhancement
21 factor since faster flow will result in a thinner (and hence smaller) ice-sheet as a result
22 of lowering the ice viscosity. An error of approximately +10% to -10% for maximum
23 ice thickness occurs between enhancement factors 1 and 5 respectively with an
24 optimum maximum ice thickness occurring between enhancement factors 2.5 and 3.
25 In contrast, the optimum enhancement factor is not reached for ice volume within the
26 limits of the range (1 to 5) investigated. The optimum enhancement factor is similar
27 for the ice volume. However, the enhancement flow factor has little effect on the ice
28 surface extent due to opposing feedbacks. Faster flow will result in an increase in the
29 flux of ice towards the ice-sheet margins. However, as the surface lowers as a result of
30 this faster flow the ablation zone will increase at the margins leading to loss of ice.
31 This result is similar to that found by Ritz et al. (1997) and Hebele et al. (2008a), in
32 terms of ice volume and maximum ice thickness. However, Hebele et al. (2008a)
33 found no increase in ice surface extent of their modelled region, comparable to results

1 shown here. In contrast, Ritz et al. (1997) found an initial slight increase in ice
2 surface extent. It is possible that this arises due to the different topography and
3 climate configurations used as hypothesised by Hebeler et al. (2008a).

4

5 There is low sensitivity of all three diagnostic skill scores to variation in the
6 geothermal heat flux. Since this influences basal temperatures of the ice-sheet it
7 affects the fluidity of the ice and the flow, as well as any basal melt. Ice velocity also
8 depends on the geothermal heat flux via the basal melt rates and in turn determines the
9 rate of sliding of the ice-sheet. This basal sliding is predicted to occur only when the
10 basal temperature is equal to the pressure melting point of ice. However, the original
11 EISMINT-3 experiment did not include basal sliding and in order for a clean
12 comparison basal sliding has also been switched off in this suite of experiments. At
13 the ice-sheet margins, the basal temperature is already at the melting point and,
14 therefore, the geothermal heat flux is not expected to influence greatly the ice volume
15 or ice surface extent. It is, therefore, more important in the central parts of the ice-
16 sheet where it could influence the flow of ice and affect the ice volume and maximum
17 ice thickness via basal melt. Ice velocity depends on the geothermal heat flux via the
18 basal melt rates and in turn determines the rate of sliding of the ice sheet. The
19 original EISMINT 3 experiment did not include basal sliding and in order for a clean
20 comparison basal sliding has also been switched off in this suite of experiments.
21 Basal sliding is predicted to occur only when the basal temperature is equal to the
22 pressure melting point of ice. Although basal temperatures in the interior are close to
23 this threshold for all cases even those, with the highest geothermal heat flux, are not
24 significant enough to cause basal melting in central parts of Greenland. This-As a
25 result the geothermal heat flux parameter is unlikely to have become more important
26 if basal sliding had been included in this suite of simulations. This is because the
27 implication of sliding concerns the outer parts of the ice-sheet where the ice base is at
28 melting point for all geothermal heat flux values investigated.- A similar result was
29 found by Hebeler et al. (2008a) for the Fennoscandian ice-sheet where very cold mean
30 annual atmospheric~~the~~ temperatures forcing was so cold resulted in very low ice
31 temperatures, As a consequence-that the influence of geothermal heat flux on the
32 thermal regime of the ice-sheet was minimal.

33

1 We also performed an experiment where the geothermal heat flux was spatially
2 varying over Greenland (Shapiro and Ritzwoller, 2004) with all other parameters set
3 at the default values. This was compared with the standard setup where the
4 geothermal heat flux was uniform over Greenland. The differences are minimal with
5 ice volume reduced by 0.32%, the ice surface extent ~~reduced-increased~~ by 0.43% and
6 the maximum ice thickness reduced by 0.1%. Since basal sliding is switched off, the
7 only effect this could have is on the basal melt and temperature of the ice at the base
8 affecting the flow by changing the viscosity of ice.

9

10 Several parameters influence the near-surface air temperature in the EISMINT-3
11 experiment, including latitudinal dependency, seasonal variation and atmospheric
12 lapse rate. Due to the PDD formulation of mass balance, these factors also directly
13 affect ablation and ice-sheet evolution. ~~Since the temperature used to force ice sheet~~
~~evolution is the near surface air temperature at the upper surface of the ice sheet, a~~
~~vertical lapse rate correction is required to take account of the ice elevation feedback.~~
~~Also important it is required to take account of the difference between the high~~
~~resolution topography seen within Glimmer (20 km), and that represented with the~~
~~forcing input data (which are on a 1° by 1° grid or approximately 111km resolution).~~
~~Glimmer currently uses a lapse rate which is not temporally or spatially varied.~~
14 Equilibrium ice surface extent increases with an increase in negative lapse rate (Fig.
15 7). A similar relationship holds for ice volume but is less pronounced. This is because
16 a less negativesmaller lapse rate results in relatively warmer near-surface air
17 temperatures at high altitude, thereby expanding the area available for ablation. The
18 eastwest negative lapse rates results in the least error but are not typical of the
19 annual lapse rate of -6.5 to $-8^{\circ}\text{C km}^{-1}$ used in several studies (e.g. Ridley et al., 2005;
20 Huybrechts and de Wolde, 1999, Vizcaino et al., 2008). However, those that use -8°C
21 km^{-1} also include a summer lapse rate. Since Glimmer only utilises one lapse rate and
22 since the majority of melting is assumed to occur during the spring/summer months a
23 summer lapse rate is justified as the input lapse rate correction in the model.
24 Maximum ice thickness is completely insensitive to lapse rate. This arises because at
25 the ice divide, where the ice thickness is highest, temperatures are already
26 significantly below zero. Any lapse rate correction will not influence the surface
27 mass balance greatly.

28

1 Maximum ice thickness is also insensitive to the PDD factors for ice and snow. This
2 is because no ablation occurs in the central part of the GrIS. However, the ice
3 surface extent is strongly affected, decreasing with increasing PDD factors. Ice
4 volume is also sensitive to the PDD factors but less pronounced than ice surface
5 extent. Although varying these parameters has an effect on melting rates it does not
6 alter the position of the ablation zones. Similar results were found by both Ritz et al.
7 (1997) and Hebeler et al. (2008a).

8

9 The results of these sensitivity experiments show which parameters control different
10 aspects of the geometry of the GrIS. Ice surface extent is fundamentally dependent on
11 those parameters which control ablation (PDD factors and lapse rate) while maximum
12 ice thickness and ice volume is controlled by parameters affecting ice flow (flow
13 enhancement factor). All three diagnostics are insensitive to variation in the
14 geothermal heat flux. From this suite of experiments it is possible to select one or
15 more parameter sets which reproduce the present day GrIS with a good fit.

16 **5.3 Selecting the optimal parameter set**

17 In order to select an optimal set of parameters which produce the best fit for present
18 day ice-sheet geometry, the 250 sensitivity experiments were ranked according to
19 each of the three diagnostics. Figure 8 shows ranking for the three absolute error skill
20 scores on the left-hand axis and the ranking for ~~NRMS~~^{normalised root mean squared}
21 ~~error~~ for ice thickness on the right-hand axis. First note that the percentage error is
22 consistently smaller for maximum ice thickness compared with ice volume and ice
23 surface extent.

24

25 We independently select a subset from the best-performing experiments for each
26 diagnostic in order to assess the effect that different parameters sets could have on
27 GrIS modelling experiments for past and future ice-sheet evolution experiments. By
28 having ~~parameter~~ set^ss which represent different aspects of the geometry of the ice-
29 sheet, some idea of the uncertainty in ice-sheet evolution can be obtained: for
30 example, future warming events. One possible way to select a subset is to arbitrarily
31 choose an ensemble size, and then choose an equal number from each diagnostics'
32 skill score. Here we use an alternative methodology which selects the best

1 performing experiments by identifying a step change in gradient in the best ranked
2 experiments, as demonstrated in the insets of Fig. 8. This removes any need for an
3 arbitrary choice and also excludes any experiments which are significantly worse but
4 selected because an equal number from each diagnostic is required. ~~Two~~^{three} experiments have been chosen according to ice volume error, ~~two~~^{four} according to ice
6 surface extent error and ~~two~~^{one} according to maximum ice thickness error. The
7 ~~three~~^{two} experiments according to normalised root mean squared ~~e~~ error for ice
8 thickness are the same as two selected for ice volume and one selected according to
9 ice surface extent. This provides ~~six~~^{eight} possible parameter ~~setups~~ which could be
10 used to model the GrIS more accurately in terms of different aspects of its geometry.

11 Figure 9 and Table 5 shows the six experiments selected and their corresponding
12 parameter values.

13
14 ~~It is important to ensure that none of these eight experiments cover the same~~
15 ~~parameter space as each other, resulting in repetition. Figure 9 shows the eight~~
16 ~~experiments selected and the distribution of their corresponding parameter values.~~
17 ~~Since there is only one experiment selected according to maximum ice thickness this~~
18 ~~will not be discounted.~~

19
20 ~~Ice surface extent has been shown to be strongly dependent on the PDD factors and~~
21 ~~lapse rate. The four chosen experiments according to this diagnostic have similar α_s~~
22 ~~values. However, one of the experiments has a lapse rate different to the other three~~
23 ~~(highlighted with a box) and is therefore selected. Two out of the three remaining~~
24 ~~experiments have similar α_s values to the one selected according to lapse rate and so~~
25 ~~are not used. This leaves two out of the four parameter setups to represent ice surface~~
26 ~~extent.~~

27
28 ~~A similar approach was applied to the three chosen ice volume experiments by~~
29 ~~discounting according to similarities in flow enhancement factor, lapse rate and PDD~~
30 ~~factors. Two out of the three experiments were selected as a result of having similar~~
31 ~~flow enhancement factors but different lapse rate and α_s values (again highlighted by~~
32 ~~boxes). Table 4 shows the final five experiments selected and their corresponding~~
33 ~~parameter values.~~

1 | Figure 10 shows how well the ~~fsixive~~ chosen parameter set~~sups~~ compare for the
2 | different diagnostic skill scores. A full unit circle would represent the experiment that
3 | out-performs all other experiments for all diagnostic skill scores. Likewise, an empty
4 | segment shows the experiment which performed worst of all experiments for that
5 | diagnostic. By comparing this measure of skill score between all 250 experiments (see
6 | Fig. 10a) four-one out of the ~~sixfive~~ chosen parameter sets perform better than average
7 | for all diagnostics (experiment 165). Those selected according to ice volume and
8 | NRMSE for ice thickness perform significantly better than average for all diagnostics
9 | apart from maximum ice thickness (experiments 10 and 233) while those selected
10 | according to maximum ice thickness (experiments 67 and 240) perform slightly below
11 | or about average for the other diagnostic. However, one experiment performs poorly
12 | for maximum ice thickness (Fig. 10a). Finally the experiment selected according to
13 | ice surface extent (experiment 99) performs better than average for all diagnostics
14 | excluding maximum ice thickness. Figure 10b shows how well each chosen
15 | experiment compares with the other selected experiments. Obviously, one will
16 | perform the worst and one the best for each diagnostic. The experiments chosen
17 | according to maximum ice thickness performs ~~worst poorly~~ for all other diagnostics,
18 | while those chosen according to ice volume and NRMSE for ice thickness perform
19 | worst for maximum ice thickness. The ~~two~~ experiments chosen according to only ice
20 | surface extent also performs poorly well for all other diagnostics while the one chosen
21 | according to ice surface extent and NRMSE ice thickness performs better than
22 | average for all diagnostics compared with the other five experiments~~maximum ice~~
23 | ~~thickness but worse for ice volume~~.

24 |
25 | Finally, the geometry of the GrIS is shown in Fig. 11 for all ~~sixfive~~ tuned parameter
26 | sets and is compared with the Bamber observation (Fig. 11a). FourAll adequately
27 | represent the limited extent of the ice-sheet in the north and west (Fig. 11b,d,e,f) but
28 | the shape of the ice-sheet in the interior is somewhat different. However, the
29 | experiments chosen according to maximum ice thickness (Fig. 11c,g) overestimate the
30 | extent of the ice-sheet in the west and the north but represent the maximum ice
31 | thickness in the interior adequately.

32 |

1 | **6 Sensitivity of the Greenland ice-sheet to tuned parameter ~~setsvalues~~**
2 | **under future warming scenarios**

3 |
4 | In order to assess how the results from tuning affect a perturbed GrIS climate from
5 | pre-industrial, we investigate the evolution of the GrIS under differing warming
6 | scenarios. This work builds on the future warming experiments described in Lunt et
7 | al. (2009). In that study, under otherwise pre-industrial boundary conditions, CO₂
8 | concentrations were perturbed from pre-industrial (280 ppmv) to 400 ppmv and 560
9 | ppmv using the GCM, HadCM3 (Gordon et al., 2000). These simulations were run
10 | for ~~a~~ time integration of 400 model years. In addition, a future warming experiment
11 | where pre-industrial CO₂ is quadrupled to 1120 ppmv was performed. However, in
12 | order to reach equilibrium a longer time integration (665 model years) was required
13 | using a version of the GCM, HadCM3L, with a lower-resolution (2.5°×3.75°
14 | compared with 1.25°×1.25° for HadCM3) ocean. The ice-sheet model set-up in Lunt
15 | et al. (2009) used ~~E~~SISMINT-3 but with ERA-40 reanalysis reference climatology for
16 | precipitation. Anomaly coupling is used to force the ice-sheet model offline. The
17 | tuneable parameters are the same as the defaults in Table 1 but with a lapse rate at -
18 | 7°C km⁻¹. We also use ERA-40 precipitation for the reference climatology but where
19 | this work differs is the use of new near-surface air temperature (modified Hanna
20 | temperature) and bedrock/ice thickness (Bamber dataset) datasets, and of course the
21 | tune~~able~~ parameter ~~setsvalues~~. Figure 12 shows the resultant configuration of the
22 | ice-sheet for the three warming scenarios. Figure 12a shows the results from Lunt et
23 | al. (2009) for comparison with the results using the optimal tuned ~~parameter~~ set~~ups~~.
24 |

25 | The original methodology with a 400 ppmv climate results in a similar ice-sheet to
26 | modern (reduced less than 2% of the modern ice-sheet). In contrast, our results using
27 | the ~~six~~^{five} optimal tuned parameter sets with the more recent boundary conditions and
28 | forcings (Fig. 12b-~~gf~~) give highly different ice-sheet configurations under a 400 ppmv
29 | climate. Although not completely collapsed, the 400 ppmv ice-sheets for Figure 12b,
30 | ~~d-f-e~~ are somewhat reduced in the north of the island, with a reduction in ice volume
31 | compared with the modern day ice-sheet volume ranging between 20 to ~~2341~~%.
32 | However, the scenario in Fig. 12~~c~~^f shows almost complete collapse at 400 ppmv with
33 | a reduction in ice volume of ~~824~~% while the scenario in Fig. 12g shows only a 5%
34 | reduction in ice volume. The main difference in parameter values between Fig. 12~~b~~^f

1 and the other four experiments is the atmospheric lapse rate which is at least $2^{\circ}\text{C km}^{-1}$
2 ~~more negative~~~~larger~~ than any of the other lapse rates chosen. During ice-sheet retreat
3 a ~~more negative~~~~higher~~ lapse rate will act to warm the region further and cause more
4 surface melt than a ~~less negative~~~~lower~~ lapse rate via the ice-elevation feedback
5 mechanism. A warmer climate compared with pre-industrial results in increased
6 melting during summer months. In all cases a ‘tipping point’ is reached whereby the
7 ice-elevation feedback results in ablation increasing relative to accumulation as the
8 ice-sheet lowers and the temperature increases. This however in the case of Fig. 12~~bf~~,
9 is re-enforced by having a ~~higher~~~~more negative~~ lapse rate value resulting in rapid loss
10 of the ice-sheet with only the highest eastern regions of the island occupied by ice.
11 However, the other experiment selected according to maximum ice thickness (Fig.
12 12g) shows almost no loss of mass under a 400 ppmv climate. Although the flow
13 enhancement factors are similar the lower PDD factors and less negative lapse rate
14 result in less melt and and no collapse of the ice-sheet.

15
16 Under a 560 ppmv climate, the GrIS is markedly reduced compared with modern with
17 a reduction in ice-sheet volume ranging from 52 to 8~~67~~%. This is not the case for the
18 set-up used in Lunt et al. (2009) where only 7% of ice mass was lost compared with
19 modern.

20
21 The further warming associated with quadrupling CO₂ concentrations results in
22 almost complete elimination of the GrIS in all cases (loss of ice volume ranging from
23 85 to 92%). This result agrees with Lunt et al. (2009), where the ice-sheet is also
24 shown to almost completely disappear apart from ice in the southern tip of the island
25 and the high eastern regions.

26
27 For the standard EISMINT-3 setup, results indicate a critical threshold for GrIS
28 collapse somewhere between 560 ppmv and 1120 ppmv. However, the new
29 ~~parameter –setsups~~ indicate a critical threshold for the GrIS becoming unstable
30 somewhere between 400 and 560 ppmv in the majority of the simulations. There is
31 also another possible threshold between pre-industrial (280 ppmv) and 400 ppmv
32 where ice is lost in the north for four out of the ~~five~~~~six~~ simulations and complete
33 collapse for one of the remaining two experiments.

34

1 Comparison can also be made with similar studies using different GCMs and/or ice-
2 sheet models. For instance, Ridley et al. (2005) showed the ice-sheet collapsed to 7%
3 of its original volume under a quadrupled CO₂ climate. The extra ice mass in our
4 simulations (1 to 8% extra) can partly be accounted for by the ice present in southern
5 Greenland which is absent in Ridley et al. (2005). This is likely due to the ice-albedo
6 feedback between climate and ice-sheet, which is included in their simulations by
7 interactive coupling of the GCM to the ice-sheet model. Interestingly the study of
8 Mikolajewicz et al. (2007) shows that under a 560 ppmv climate using a fully coupled
9 climate ice-sheet model the GrIS could result in significant melting in the long-term
10 (simulation only carried out for 600 years). Furthermore, Alley et al. (2005) showed
11 that under a doubled CO₂ climate the GrIS would eventually almost completely
12 disappear.

13

14 **7 Discussion and Conclusions**

15

16 In this section we discuss the sources of uncertainty and the missing processes in the
17 experimental design and the influence this has on the conclusions drawn. We evaluate
18 the sensitivity to boundary conditions and climate forcings in the context of modelling
19 the evolution of the GrIS under present day, steady state conditions and show the
20 geometry and size of the ice sheet is highly sensitive to the initial condition of
21 bedrock and ice thickness. An ice sheet volume 13.7% larger than that produced with
22 the Letreguilly dataset results with the new and improved Bamber dataset. Overall,
23 our study indicates that using the more recent datasets for forcings and boundary
24 conditions with the standard set of model parameters (Table 4) give a poor
25 representation of the modern ice sheet, with an ice sheet volume 25% larger than
26 observation.

27

28 Several parameters are not well constrained in large scale ice sheet modelling and can
29 influence ice sheet volume and extent. We performed a sensitivity/tuning study in
30 order to assess the importance of certain parameters on the geometry and size of the
31 GrIS. The method of LHS was used in order to efficiently vary more than one
32 parameter at a time to obtain a best fit between modelled and observed geometry. The
33 maximum ice thickness and ice volume were shown to depend on the factors affecting
34 ice flow; in this case the flow enhancement factor where the faster the flow the lower

1 the ice dome. The ice surface extent is predominantly dependent on the PDD factors
2 and the atmospheric lapse rate. Although geothermal flux can affect ice flow since it
3 acts to melt the ice, which is a prerequisite for basal sliding, this had little effect on
4 the simulations presented here because basal sliding was switched off.

5
6 By selecting ‘best fit’ experiments according to different skill score diagnostics and
7 further sub-selection according to the spread in parameter values, a range of parameter
8 sets can be used for assessing the uncertainty in ice sheet modelling experiments by
9 analysing the resultant geometries. The sets of parameters that give the best fit to the
10 present measured ice sheet are somewhat different from the standard set most
11 commonly used by ice sheet modelling studies. High PDD factors (16.0 to 19.5 mm
12 $\text{d}^{+} \text{C}^{+}$ for α_r and 3.6 to 4.9 mm $\text{d}^{+} \text{C}^{+}$ for α_s) are required in all cases in order to
13 account for both ablation and calving processes at the margin. Furthermore, low
14 atmospheric lapse rates (four out of the five tuned setups ranged between 4.0 and
15 $5.3 \text{ }^{\circ}\text{C km}^{-1}$) are generally needed to produce a good fit in terms of volume by
16 reducing the growth of the ice sheet. Higher flow enhancement factors (e.g. 4.9 when
17 α_r is 0.16) are required if the ablation coefficients are reduced in order to compensate
18 mass loss by simulating faster flow.

19
20 The optimal parameter sets chosen to best represent the modern day GrIS sheet were
21 used to assess their affect on the evolution of the ice sheet under future warming
22 scenarios. We obtained a different threshold for ice sheet collapse, occurring
23 somewhere between 400 ppmv and 560 ppmv compared with previous work which
24 suggested a threshold between 560 and 1120 ppmv (Lunt et al., 2009) when using the
25 same models. Differences in ice sheet geometry and volume also occur between the
26 optimal parameter setups. Although all ice sheets were similar for present day, one
27 particular set (Table 4, experiment 230) showed complete collapse at 400 ppmv. We
28 show under perturbed climates from present day the evolution of the GrIS behaves
29 differently for the parameter sets tuned in the model. This work suggests that, if
30 possible, tuning exercises should be applied to the GrIS under several different
31 climatologies. Since observations are required for comparison this is somewhat
32 restrictive. However, examples of alternative climates to the present day could be the
33 last deglaciation or the Last Glacial Maximum, for which there exist some data on ice-
34 sheet extent.

1 Firstly, several other temperature datasets over Greenland exist to force the Glimmer
2 ice-sheet model. A new parameterisation based on more up-to-date Automatic
3 Weather Station data, for instance, is now available with a similar form to Eq. (6) and
4 Eq. (7) (Fausto et al., 2009). However, we chose the novel approach to use original
5 temperature observations rather than a highly tuned parameterisation. Furthermore,
6 datasets also exist in terms of satellite products. For satellite datasets, temperature
7 data are available from the Advanced Very High Resolution Radiometer (AVHRR)
8 Polar Pathfinder (APP) from 1982 – 2004 which is collated twice a day at the local
9 solar times of 1400 and 0400. Although the data is initially on a 5 km resolution it is
10 sub-sampled at 25 km pixels. The APP-x product includes all-sky surface temperature
11 with the cloudy-sky surface temperatures calculated using an empirical relationship
12 between clear-sky surface temperature, wind speed, and solar zenith angle (daytime).
13 However, this only applies to surface temperatures over sea-ice and not land.
14 Therefore, temperatures over Greenland are based only on data from clear-sky
15 retrieval with temperatures in cloudy regions interpolated from clear-sky areas.
16 Although useful for comparing with present day surface temperatures from climate
17 models, this dataset is not suitable to directly force an ice-sheet model over Greenland
18 because a) the largest uncertainties are likely to be over Greenland (Key, pers.
19 comm.), b) no associated orography exists which is used to downscale from the
20 resolution of the forcing data onto the high-resolution of the ice-sheet model. And c)
21 sensitivity studies using Glimmer indicate that the APP-x temperatures were
22 significantly too cold, in observed ice-free regions such as western Greenland, (by up
23 to 12°C in western Greenland compared with EISMINT-3 temperatures which have at
24 least been derived from surface observation) to reproduce a reasonable modern day
25 ice-sheet without tuning ice-sheet model parameters beyond uncertainty ranges. This
26 could, in part, be due to the satellite recording ice surface temperatures rather than air
27 temperature. Furthermore, clear-sky retrievals errors are predominantly due to
28 uncertainties in cloud detection (Key et al., 1997) particularly during the night. The
29 low temperatures, bright surface and high elevation make remote sensing over
30 Greenland particularly difficult in terms of accurate cloud detection.

31
32 Secondly, in contrast to many studies, we spin up the model from present day
33 initial conditions without taking the climate history into account. Since the GrIS is
34 still affected by past climatic change this assumption must be justified. The main

1 method used to spin up the ice-sheet model over several climatic cycles has caveats of
2 its own. It uses a temperature forcing derived from a smoothed ice core record and has
3 been used in several studies (e.g. Huybrechts and de Wolde, 1999; Ridley et al., 2005;
4 Vizcaino et al., 2008). However, uncertainty exists in the functions used to derive a
5 reliable temperature record and subsequent accumulation record from an oxygen
6 isotopic record although new, more and sophisticated methods are being developed
7 (Cuffey and Marshall, 2000; Lhomme et al., 2005). The effect of ice flow processes on
8 deeper parts of ice cores also makes them somewhat unreliable and extending beyond
9 the last interglacial is somewhat unrealistic (Grootes et al., 1993; Johnsen et al.,
10 1997). For these reasons we only initiate [the ice-sheet model](#) from the present day
11 initial conditions, which we can be certain are relatively accurate.

12

13 [Thirdly, the process of basal sliding was not included in the experimental design,](#)
14 [which has implications for the amount of ice mass lost dynamically. An increase in](#)
15 [the ice velocity, by incorporating the sliding velocity \(see Eq. 2\), would result in more](#)
16 [ice transferred from the accumulation zone to the ablation zone and, therefore, reduce](#)
17 [the volume of the ice-sheet. Inclusion of this missing process could result in lower](#)
18 [PDD factors than those obtained in the tuning exercise presented here. Indeed, the](#)
19 [study by Parizek and Alley \(2004\) showed an increase in GrIS sensitivity to various](#)
20 [warming scenarios due to surface meltwater lubrication of flow. Recent modelling](#)
21 [developments have also investigated the potential positive feedbacks from including](#)
22 [basal sliding on the inland migration of fast-flowing glaciers increasing the drawdown](#)
23 [of the ice-sheet interior \(e.g. Price et al., 2008\). Currently, Glimmer has a simplified](#)
24 [representation of basal sliding and the basal hydrology. Furthermore, there is no](#)
25 [representation of the sediment deformation. The presence of unconsolidated](#)
26 [sediments alters the hydrological system by incorporating melt water until saturation](#)
27 [is reached. This reduces the yield stress of the material substantially and deformation](#)
28 [of the basal till by the overlying ice load inducing glacier motion. However studies](#)
29 [have mainly focussed on the local scale of ice streams rather than the continental scale](#)
30 [of ice-sheets \(Tulaczyk et al., 2000; Sayag and Tziperman, 2008\).](#)

31

32 [Fourthly, Current current](#) ice-sheet models lack higher-order physics, and although
33 able to simulate slow moving ice dynamics adequately, they are not yet able to
34 represent the dynamics of fast-moving ice streams. Recent work has indicated that

1 current net mass loss from-of mass from the GrIS is roughly equally partitioned
2 between surface mass balance changes and changes in dynamics (van den Broeke et
3 al., 2009). Development of ice-sheet models in these areas is currently being
4 researched with improvements to ice dynamics (e.g. Soucek and Martinec, 2008;
5 Pattyn, 2003), and inclusion of an accurate representation of the fast ice streams and
6 ice shelves (Pattyn et al., 2006; Schoof, 2006; Schoof, 2007). Recent observations of
7 glaciers in Greenland have documented rapid changes in marginal regions of the ice-
8 sheet with increased flow velocities observed on Jakobshavn Glacier (Joughin et al.,
9 2004) and on other glaciers (e.g. Howat et al., 2007; Rignot and Kanagaratnam,
10 2006). The inclusion of these fast flowing ice streams in ice-sheet models could lead
11 to larger dynamical changes in the ice-sheet than currently predicted by models at
12 least on relatively short timescales of hundreds of years. Incorporation of these fast
13 flow features in the ice-sheet model could also result in lower PDD factors from
14 tuning. Furthermore, if these dynamical changes are marine-driven then for long-term
15 future ice-sheet predictions, once the ice-streams are no longer marine terminating,
16 the dynamical changes will cease.

17

18 It has also been shown that processes at the ice margin have a strong influence on the
19 surface extent of the ice-sheet but are poorly accounted for with a coarse grid of 20-
20 km resolution. The use of energy-balance/snow pack models (EBSM) to predict
21 surface mass balance (e.g. Bougamont et al., 2007) as opposed to the PDD approach
22 has been shown to give contrasting results under a 4 times CO₂ climate with the PDD
23 scheme significantly more sensitive to a warming climate generating runoff rates
24 almost twice as large compared with an EBSM. However, some aspects of these
25 results are not undisputed (Huybrechts 2009, pers. comm.). The ablation zone on
26 Greenland varies from only 1-km wide along the southeast coast and up to 150-km
27 wide along the southwest coastline and, therefore, requires a very high horizontal
28 resolution if ablation is not to be over or underestimated in the model (Van den
29 Broeke, 2008). Future development of the EBSM approach using a finer grid of 5-km
30 resolution could result in a marked improvement for modelling ablation processes. It
31 would also be highly beneficial to downscale to a 1x1-km resolution using a PDD
32 approach (e.g. Janssens and Huybrechts, 2000) and the high-resolution Greenland
33 DEMs now available (e.g. Bamber et al. 2001).

34

1 An alternative to the finite difference modelling approach used here could be to
2 instead implement the finite element modelling method. This has the advantage that
3 the element size can be reduced in areas of high gradient and increased in areas of low
4 gradient. Furthermore, the model can conform to irregular boundaries that are
5 awkward to model with rectangular elements used in the finite differences technique.
6 Currently this methodology is used over smaller domains such as individual glaciers
7 (e.g. Zwinger et al., 2007) or within flow line models of ice-sheets (e.g. Parizek,
8 2005).

9
10 Overcoming the abstraction required for large scale ice-sheet models, in order to keep
11 computing demands to a minimum while ensuring spatial variability at the sub-scale
12 level is captured, subgrid parameterisations for the calculation of
13 ablation/accumulation has been shown to be effective (Marshall and Clark, 1999;
14 Hebeler and Purves, 2008b).

15
16 We evaluate the sensitivity to boundary conditions and climate forcings in the context
17 of modelling the evolution of the GrIS under present day, steady-state conditions and
18 show the geometry and size of the ice-sheet is highly sensitive to the initial condition
19 of bedrock and ice thickness. An ice-sheet volume 13.7% larger than that produced
20 with the Letreguilly dataset results with the new and improved Bamber dataset.
21 Overall, our study indicates that using the more recent datasets for forcings and
22 boundary conditions with the standard set of model parameters (Table 1) give a poorer
23 representation of the modern ice-sheet, with an ice-sheet volume 33% larger than
24 observation. The results further show that topography and its inherent uncertainty has
25 a significant effect on ice-sheet geometry obtained from large scale models of
26 considerable abstraction such as Glimmer. Therefore, the use of more realistic
27 topography and climate data on an original resolution significantly higher than that
28 used in Glimmer may not be entirely suitable for current large scale ice-sheet
29 modelling.

30
31 Several parameters are not well-constrained in large-scale ice-sheet modelling and can
32 influence ice-sheet volume and extent. We performed a sensitivity/tuning study in
33 order to assess the importance of certain parameters on the geometry and size of the
34 GrIS. The method of LHS was used in order to efficiently vary more than one

1 parameter at a time to obtain a best fit between modelled and observed geometry. The
2 maximum ice thickness and ice volume were shown to depend on the factors affecting
3 ice flow. In this case increasing the flow enhancement factor makes the ice flow faster
4 which lowers the height of the ice dome. The ice surface extent is predominantly
5 dependent on the PDD factors and the atmospheric lapse rate. Although geothermal
6 flux can affect ice flow since it acts to melt the ice, which is a prerequisite for basal
7 sliding, this had little effect on the simulations presented here because basal sliding
8 was switched off.

9

10 By selecting ‘best fit’ experiments according to different skill score diagnostics a
11 range of parameter sets can be used for assessing the uncertainty in ice-sheet
12 modelling experiments by analysing the resultant geometries. The sets of parameters
13 that give the best fit to the present measured ice-sheet are somewhat different from the
14 standard set most commonly used by ice-sheet modelling studies. Higher PDD
15 factors than the standard (10.2 to 19.9 $\text{mm d}^{-1} \text{C}^{-1}$ for α_i and 3.6 to 4.8 $\text{mm d}^{-1} \text{C}^{-1}$ for
16 α_s) are required in all cases in order to account for both ablation and calving processes
17 at the margin. The lack of basal sliding in these simulations means that these higher
18 PDD factors are likely partially compensating for this missing process. Furthermore,
19 less negative atmospheric lapse rates (five out of the six tuned parameter sets ranged
20 between -4.1 and -6.0 $^{\circ}\text{C km}^{-1}$) are generally needed to produce a good fit in terms of
21 volume by reducing the growth of the ice-sheet.

22

23 The parameters varied using LHS are strictly independent in a mathematical sense.
24 However, it is possible that the values chosen could have similar and opposite effects
25 on accurately predicting the present day GrIS geometry. For example, high PDD
26 factors in combination with low lapse rates could simulate a good representation of
27 the GrIS. In our conclusions we do not attempt to make a probabilistic interpretation
28 of the results such that certain combinations are more likely than others in producing
29 an accurate representation of the ice-sheet.

30

31 The optimal parameter sets chosen to best represent the modern day GrIS were used
32 to assess their effect on the evolution of the ice-sheet under future warming scenarios.
33 We obtained a different threshold for ice-sheet collapse, occurring somewhere
34 between 400 ppmv and 560 ppmv compared with previous work which suggested a

1 threshold between 560 and 1120 ppmv (Lunt et al., 2009) when using the same
2 models. Differences in ice-sheet geometry and volume also occur between the
3 optimal parameter sets. Although all ice-sheets modelled for present day showed
4 complete glaciation of Greenland, one particular parameter set (Table 5, experiment
5 67) showed complete collapse at 400 ppmv. We show under perturbed climates from
6 present day the evolution of the GrIS behaves differently for the parameter sets tuned
7 in the model. This work suggests that, if possible, tuning exercises should be applied
8 to the GrIS under several different climatologies. Since observations are required for
9 comparison this is somewhat restrictive. However, examples of alternative climates to
10 the present day could be the last deglaciation or the Last Glacial Maximum, for which
11 there exist some data on ice-sheet extent.

12
13 We have shown that future predictions of the GrIS are highly sensitive to a number of
14 factors relating to the physical basis of the ice-sheet model. Current models neither
15 have a robust representation of the fast flowing processes, nor are the parameters
16 which influence the ice physics tightly constrained. As a result future development of
17 the ice-sheet model to improve the representation of these processes may lead to
18 different behaviour under warm climate conditions. In conclusion, The lack of
19 higher-order physics, low resolution, absence of basal sliding and subglacial
20 hydrology and highly parameterised surface balance, inevitably means that the tuning
21 presented here compensates for these absent processes in order to replicate as closely
22 as possible the present day GrIS. As a result, future predictions of the GrIS should be
23 aired with some caution in the context of these sensitivities and deficiencies of the
24 ice-sheet model.

27 **Acknowledgements**

28 This work was supported by the Natural Environmental Council. EH thanks the
29 British Atmospheric Data Centre for provision of ECMWF/ERA-40 (re)analysis data
30 and Philippe Huybrechts for supplying the 5x5-km Greenland DEM. ES thanks
31 Patrick Applegate for helpful discussions concerning the forcing data used.

1 **References**

2 Alley, R. B., Clark, P. U., Huybrechts, P., and Joughin, I.: Ice-Sheet and Sea-Level
3 Changes. *Science*, 310, 456-460, 2005.

4 Bamber, J. L., Layberry, R. L., and Gogineni, P.: A new ice thickness and bed data set
5 for the Greenland ice-sheet 1. Measurement, data reduction, and errors. *J. Geophys.*
6 *Res.*, 106, 33773-33780, 2001.

7 Banks, D. *An Introduction to Thermogeology Ground Source Heating and Cooling*,
8 Blackwell Publishing Ltd, Oxford, UK, 339pp., 2008.

9 Bougamont, M., Bamber, J. L., Ridley, J. K., Gladstone, R. M., Greuell, W., Hanna,
10 E., Payne, A. J., and Rutt, I.: Impact of model physics on estimating the surface mass
11 balance of the Greenland ice-sheet. *Geophys. Res. Lett.*, 34, L17501,
12 doi:10.1029/2007GL030700, 2007.

13 Braithwaite, R. J.: Positive degree-day factors for ablation on the Greenland ice-sheet
14 studied by energy-balance modelling. *J. Glaciol.*, 41, 153-160, 1995.

15 Bromwich, D. H., Cullather, R. I., Chen, Q., and Csatho, B. M.: Evaluation of recent
16 precipitation studies for Greenland ice-sheet. *J. Geophys. Res.-Atmos.*, 103, 26007-
17 26024, 1998.

18 Buchardt, S. L., and Dahl-Jensen, D.: Estimating the basal melt rate at NorthGRIP
19 using a Monte Carlo technique. *Ann. Glaciol.*, 45, 137-142, 2007.

20

21 Burgess, E. W., Forster, R. R., Box, J. E., Smith, L. C., and Bromwich, D. H.:
22 Greenland ice-sheet annually-resolved accumulation rates (1958-2007), a Spatially
23 Calibrated Model. *J. Geophys. Res.*, provisionally accepted, 2009.

24 Calov, R., and Hutter, K.: The thermomechanical response of the Greenland ice-sheet
25 to various climate scenarios. *Clim. Dynam.*, 12, 243-260, 1996.

26 Cuffey, K. M., and Marshall, S. J.: Substantial contribution to sea-level rise during the
27 last interglacial from the Greenland ice-sheet. *Nature*, 404, 591-594, 2000.

1 Dahl-Jensen, D., and Johnsen, S. J.: Paleotemperatures Still Exist in the Greenland
2 Ice-Sheet. *Nature*, 320, 250-252, 1986.

3 Dahl-Jensen, D., and Gundestrup, N. S.: Constitutive properties of ice at Dye 3,
4 Greenland. In: *The Physical Basis of Ice Sheet Modelling*, International Association
5 of Hydrological Sciences Publ., 170, 31-43, 1987.

6 DeConto, R. M., and Pollard, D.: Rapid Cenozoic glaciation of Antarctica induced by
7 declining atmospheric CO₂. *Nature*, 421, 245-249, 2003.

8 Driesschaert, E., Fichefet, T., Goosse, H., Huybrechts, P., Janssens, I., Mouchet, A.,
9 Munhoven, G., Brovkin, V., and Weber, S.L. : Modeling the influence of Greenland
10 ice-sheet melting on the Atlantic meridional overturning circulation during the next
11 millennia. *Geophys. Res. Lett.*, 34, L10707, doi:10.1029/2007GL029516, 2007.

12 ECMWF. ECMWF ERA-40 Re-Analysis data.[Internet]. British Atmospheric Data
13 Centre, 2006: <http://badc.nerc.ac.uk/data/ecmwf-e40/>, access: March 13 2009.

14 Edwards, N., and Marsh, R.: Uncertainties due to transport-parameter sensitivity in an
15 efficient 3-D ocean-climate model. *Clim. Dynam.*, 24, 415-433, 2005.

16 Ekholm, S.: A full coverage, high-resolution topographic model of Greenland
17 computed from a variety of digital elevation data. *J. Geophys. Res.*, 101, 21961-
18 21972, 1996.

19 Essery, R., and Etchevers, P.: Parameter sensitivity in simulations of snowmelt. *J.*
20 *Geophys. Res.-Atmos.*, 109, D20111, doi:10.1029/2004JD005036, 2004.

21 Ettema, J. Van den Broeke, M. R., Van Meijgaard, E., Van de Berg, W. J., Bamber,
22 J.L., Box, J. E., and Bales, R. C.: Higher surface mass balance of the Greenland ice-
23 sheet revealed by high-resolution climate modeling. *Geophys. Res. Lett.*, 36, L12501,
24 doi:10.1029/2009GL038110, 2009.

25

1 Fabre, A., Letreguilly, A., Ritz, C., and Mangeney, A.: Greenland under changing
2 climates: sensitivity experiments with a new three-dimensional ice-sheet model. *Ann.*
3 *Glaciol.*, 21, 1-7, 1995.

4 Fausto, R. S., Ahlstrom, A. P., Van As, D., Boggild, C. E., and Johnsen, S. J.: A new
5 present-day temperature parameterisation for Greenland. *J. Glaciol.*, 55, 95-105,
6 2009.

7 Fichefet, T., Poncin, C., Goosse, H., Huybrechts, P., Janssens, I., and Le Treut, H.:
8 Implications of changes in freshwater flux from the Greenland ice-sheet for the
9 climate of the 21st century. *Geophys. Res. Lett.*, 30, 17, 1911,
10 doi:10.1029/2003GL017826, 2003.

11 Glover, R. W.: Influence of spatial resolution and treatment of orography on GCM
12 estimates of the surface mass balance of the Greenland ice-sheet. *J. Climate*, 12, 551-
13 563, 1999.

14 Gordon, C., Cooper, C., Senior, C. A., Banks, H., Gregory, J., Johns, T. C., Mitchell,
15 J. F. B., and Wood, R. A.: The simulation of SST, sea ice extents and ocean heat
16 transports in a version of the Hadley Centre coupled model without flux adjustments.
17 *Clim. Dynam.*, 16, 147-168, 2000.

18 Gregory, J. M., and Huybrechts, P.: Ice-sheet contributions to future sea-level change.
19 *Philos. T. R. Soc. A*, 364, 1709-1731, 2006.

20 Greve, R., and Hutter, K.: Polythermal three-dimensional modelling of the Greenland
21 ice-sheet with varied geothermal heat flux. *Ann. Glaciol.*, 21, 8-12, 1995.

22 Greve, R.: On the response of the Greenland ice-sheet to greenhouse climate change.
23 *Climatic Change*, 46, 289-303, 2000.

24 Greve, R.: Relation of measured basal temperatures and the spatial distribution of the
25 geothermal heat flux for the Greenland ice-sheet. *Ann. Glaciol.*, 42, 424-432, 2005.

1 Grootes, P. M., Stuiver, M., White, J. W. C., Johnsen, S., and Jouzel, J.: Comparison
2 of Oxygen-Isotope Records from the Gisp2 and Grip Greenland Ice Cores. *Nature*,
3 366, 552-554, 1993.

4 Hanna, E., and Valdes, P.: Validation of ECMWF (re)analysis surface climate data,
5 1979-1998, for Greenland and implications for mass balance modelling of the Ice-
6 sheet. *Int. J. Climatol.*, 21, 171-195, 2001.

7 Hanna, E., Huybrechts, P. Janssens, I., Cappelen, J., Steffen, K., and Stephens, A.:
8 Runoff and mass balance of the Greenland ice-sheet: 1958-2003. *J. Geophys. Res.-*
9 *Atmos.*, 110, D13108, doi:10.1029/2004JD005641, 2005.

10 Hanna, E., McConnell, J., Das, S., Cappelen, J., and Stephens, A.: Observed and
11 modeled Greenland ice-sheet snow accumulation, 1958-2003, and links with regional
12 climate forcing. *J. Climate*, 19, 344-358, 2006.

13 Hanna, E., Huybrechts, P., Steffen, K., Cappelen, J., Huff, R., Shuman, C., Irvine-
14 Fynn, T., Wise, S., and Griffiths, M.: Increased runoff from melt from the Greenland
15 Ice-sheet: A response to global warming. *J. Climate*, 21, 331-341, 2008.

16 Hebeler, F., Purves, R. S., and Jamieson, S. S. R.: The impact of parametric
17 uncertainty and topographic error in ice-sheet modelling. *J. Glaciol.*, 54, 899-919,
18 2008a.

19 Hebeler, F., and Purves, R. S.: The influence of resolution and topographic
20 uncertainty on melt modelling using hypsometric sub-grid parameterization. Hydrol.
21 Process., 22, 19, 3965-3979, 2008b.

22 Howat, I. M., Joughin, I., and Scambos, T. A.: Rapid changes in ice discharge from
23 Greenland outlet glaciers. *Science*, 315, 1559-1561, 2007.

25 Huybrechts, P., Letreguilly, A., and Reeh, N.: The Greenland Ice-Sheet and
26 Greenhouse Warming. *Global Planet. Change*, 89, 399-412, 1991.

1 Huybrechts, P., and Payne, A. J.: The EISMINT benchmarks for testing-ice-sheet
2 models. *Ann. Glaciol.*, 23, 1-12, 1996.

3 Huybrechts, P.: Report of the Third EISMINT Workshop on Model Intercomparison.
4 Grindelwald, Switzerland, 25-27 September 1997.

5 Huybrechts, P., and de Wolde, J.: The dynamic response of the Greenland and
6 Antarctic ice-sheets to multiple-century climatic warming. *J. Climate*, 12, 2169-2188,
7 1999.

8 IPCC. Climate Change 2007: The Physical Sciences Basis. Contribution of Working
9 Group I to the Fourth Assessment Report of the Intergovernmental Panel on Climate
10 Change . Solomon, S., Qin, D., Manning, M., Chen, Z., Marquis, M., Averyt, K. B.,
11 Tignor, M., and Miller, H. L. (Eds). Cambridge University Press, Cambridge, United
12 Kingdom and New York, NY, USA, 2007.

13 Janssens, I., and Huybrechts, P.: The treatment of meltwater retention in mass-balance
14 parameterizations of the Greenland ice-sheet. *Ann. Glaciol.*, 31, 133-140, 2000.

15 Johnsen, S. J., Clausen, H. B., Dansgaard, W., Gundestrup, N. S., Hammer, C. U.,
16 Andersen, U., Andersen, K. K., Hvidberg, C. S., Dahl-Jensen, D., Steffensen, J. P.,
17 Shoji, H., Sveinbjörnsdóttir, A. E.: The delta O-18 record along the Greenland Ice
18 Core Project deep ice core and the problem of possible Eemian climatic instability. *J.*
19 *Geophys. Res.-Oceans*, 102, C12, 26397-26410, 1997.

20 Joughin, I., Abdalati, W., and Fahnestock, M.: Large fluctuations in speed on
21 Greenland's Jakobshavn Isbrae glacier. *Nature*, 432, 608-610, 2004.

22 Key, J. R., Schweiger, A. J., and Stone, R. S.: Expected uncertainty in satellite-
23 derived estimates of the surface radiation budget at high latitudes. *J. Geophys. Res.-*
24 *Oceans*, 102, C7, 15837-15847, 1997.

25 Lambeck, K., and Nakiboglu, S. M.: Seamount Loading and Stress in the Ocean
26 Lithosphere. *J. Geophys. Res.*, 85, 6403-6418, 1980.

1 Lee, W. H. K.: On the global variations of terrestrial heat flow. *Phys. Earth Planet.*
2 *Interiors*, 2, 332-341, 1970.

3 Lefebvre, F., Gallee, H., Van Ypersele, J. P., and Huybrechts, P.: Modelling of large-
4 scale melt parameters with a regional climate model in south Greenland during the
5 1991 melt season. *Ann. Glaciol.*, 35, 391-397, 2002.

6 Letreguilly, A., Huybrechts, P., and Reeh, N.: Steady-State Characteristics of the
7 Greenland Ice-Sheet under Different Climates. *J. Glaciol.*, 37, 149-157, 1991.

8 Lhomme, N., Clarke, G. K. C., and Marshall, S. J.: Tracer transport in the Greenland
9 Ice-sheet: constraints on ice cores and glacial history. *Quaternary Sci. Rev.*, 24, 173-
10 194, 2005.

11 Luckman, A., Murray, T., de Lange, R., and Hanna, E.: Rapid and synchronous ice-
12 dynamic changes in East Greenland. *Geophys. Res. Lett.*, 33, L03503,
13 doi:10.1029/2005GL025428, 2006.

14 Lunt, D. J., Foster, G. L., Haywood, A. M., and Stone, E. J.: Late Pliocene Greenland
15 glaciation controlled by a decline in atmospheric CO₂ levels. *Nature*, 454, 1102-1105,
16 2008.

17 Lunt, D. J., Haywood, A. M., Foster, G. L., and Stone, E. J.: The Arctic cryosphere in
18 the Mid-Pliocene and the future. *Philos. T. R. Soc. A*, 367, 49-67, 2009.

19 Marshall, S. J., and Clarke, G. K. C.: Ice sheet inception: subgrid hypsometric
20 parameterization of mass balance in an ice sheet model. *Clim. Dynam.*, 15, 7, 533-
21 550, 1999.

22 McKay, M. D., Beckman, R. J., and Conover, W. J.: A Comparison of Three Methods
23 for Selecting Values of Input Variables in the Analysis of Output from a Computer
24 Code. *Technometrics*, 21, 239-245, 1979.

1 Mikolajewicz, U., Gröger, M., Maier-Reimer, E., Schrgers, G., Vizcaíno, M., and
2 Winguth, A. M. E.: Long-term effects of anthropogenic CO₂ emissions simulated with
3 a complex earth system model. *Clim. Dynam.*, 28, 599-631, 2007.

4 Murphy, C., Fealy, R., Charlton, R., and Sweeney, J.: The reliability of an 'off-the-
5 shelf' conceptual rainfall runoff model for use in climate impact assessment:
6 uncertainty quantification using Latin hypercube sampling. *Area*, 38, 65-78, 2006.

7 NGRIP: High-resolution record of Northern Hemisphere climate extending into the
8 last interglacial period. *Nature*, 431, 147-151, 2004.

9 Ohmura, A.: New temperature distribution maps for Greenland. *Z. Gletscherkd.*
10 *Glazialgeol.*, 23, 1-45, 1987.

11 Ohmura, A., and Reeh, N.: New Precipitation and Accumulation Maps for Greenland.
12 *J. Glaciol.*, 37, 140-148, 1991.

13 Parizek, B. R. and Alley, R. B.: Implications of increased Greenland surface melt
14 under global-warming scenarios: ice-sheet simulations. *Quaternary Sci. Rev.*, 23, 9-
15 10, 1013-1027, 2004.

16

17 Parizek, B. R., Alley, R. B. and MacAyeal, D. R.: The PSU/UofC finite-element
18 thermomechanical flowline model of ice-sheet evolution *Cold Reg. Sci. Technol.*, 42,
19 145-168, 2005.

20

21 Pattyn, F.: A new three-dimensional higher-order thermomechanical ice-sheet model:
22 Basic sensitivity, ice stream development, and ice flow across subglacial lakes. *J.*
23 *Geophys. Res.- Sol. Ea.*, 108, B8, 2382, doi:10.1029/2002JB002329, 2003.

24 Pattyn, F., Huyghe, A., De Brabander, S., and De Smedt, B.: Role of transition zones
25 in marine ice-sheet dynamics. *J. Geophys. Res.-Earth*, 111, F02004,
26 doi:10.1029/2005JF000394, 2006.

1 Payne, A. J.: A thermomechanical model of ice flow in West Antarctica. *Clim.*
2 *Dynam.*, 15, 115-125, 1999.

3 Pollard, D., and Thompson, S. L.: Driving a high-resolution dynamic ice-sheet model
4 with GCM climate: ice-sheet initiation at 116,000BP. *Ann. Glaciol.*, 25, 296-304,
5 1997.

6 Price, S. F., Conway, H., Waddington, E. D. and Bindschadler, R. A.: Model
7 investigations of inland migration of fast-flowing outlet glaciers and ice streams. J.
8 Glaciol., 54, 184, 49-60.

9

10 Reeh, N.: Parameterization of melt rate and surface temperature on the Greenland ice-
11 sheet. *Polarforschung*, 59, 113-128, 1991.

12 Ridley, J. K., Huybrechts, P., Gregory, J. M., and Lowe, J. A.: Elimination of the
13 Greenland ice-sheet in a high CO₂ climate. *J. Climate*, 18, 3409-3427, 2005.

14 Rignot, E., and Kanagaratnam, P.: Changes in the velocity structure of the Greenland
15 ice-sheet. *Science*, 311, 986-990, 2006.

16 Rignot, E., Box, J. E., Burgess, E., and Hanna, E.: Mass balance of the Greenland ice-
17 sheet from 1958 to 2007. *Geophys. Res. Lett.*, 35, L20502,
18 doi:10.1029/2008GL035417, 2008.

19 Ritz, C.: Time dependent boundary conditions for calculation of temperature fields in
20 ice-sheets. In: *The Physical Basis of Ice-sheet Modelling*, International Association of
21 Hydrological Sciences Publ., 170, 207-216, 1987.

22 Ritz, C., Fabre, A., and Letreguilly, A.: Sensitivity of a Greenland ice-sheet model to
23 ice flow and ablation parameters: Consequences for the evolution through the last
24 climatic cycle. *Clim. Dynam.*, 13, 11-24, 1997.

25 Rutt, I. C., Haggdorn, M., Hulton, N. R. J., and Payne, A. J.: The Glimmer community
26 ice-sheet model. *J. Geophys. Res.-Earth*, 114, F02004, doi:10.1029/2008JF001015,
27 2009.

1 [Sayag, R. and Tziperman, E.: Spontaneous generation of pure ice streams via flow](#)
2 [instability: Role of longitudinal shear stresses and subglacial till, J. Geophys. Res.-](#)
3 [Earth, 113, B05411, doi:10.1029/2007JB005228.](#)

4

5 Schneider von Deimling, T., Held, H., Ganopolski, A., and Rahmstorf, S.: Climate
6 sensitivity estimated from ensemble simulations of glacial climate. *Clim. Dynam.*, 27,
7 149-163, 2006.

8 Schoof, C.: A variational approach to ice stream flow. *J. Fluid Mech.*, 556, 227-251,
9 2006.

10 Schoof, C.: Ice-sheet grounding line dynamics: Steady states, stability, and hysteresis.
11 *J. Geophys. Res.-Earth*, 112, F03S28, doi:10.1029/2006JF000664, 2007.

12 Serreze, M. C., and Hurst, C. M.: Representation of mean Arctic precipitation from
13 NCEP-NCAR and ERA reanalyses. *J. Climate*, 13, 182-201, 2000.

14 Serreze, M. C., Barrett, A., P., and Lo, F.: Northern High-Latitude Precipitation as
15 Depicted by Atmospheric Reanalyses and Satellite Retrievals. *Mon. Weather Rev.*,
16 133, 3407-3430, 2005.

17 Shapiro, N. M., and Ritzwoller, M. H.: Inferring surface heat flux distributions guided
18 by a global seismic model: particular application to Antarctica. *Earth Planet. Sc. Lett.*,
19 223, 213-224, 2004.

20 Soucek, O., and Martinec, Z.: Iterative improvement of the shallow-ice
21 approximation. *J. Glaciol.*, 54, 812-822, 2008.

22 Steffen, K., and Box, J.: Surface climatology of the Greenland ice-sheet: Greenland
23 Climate Network 1995-1999. *J. Geophys. Res.*, 106, D24, 33951-33964, 2001.

24 [Tulaczyk, S., Kamb, W. B. and Engelhardt, H. F.: Basal mechanics of Ice Stream B,](#)
25 [West Antarctica 2. Undrained plastic bed model. J. Geophys. Res.-Earth, 105, B1,](#)
26 [483-494, 2000.](#)

27

1 Uppala, S. M., Kållberg, P. W., Simmons, A. J., Andrae, U., Da Costa Bechtold, V.,
2 Fiorino, M., Gibson, J. K., Haseler, J., Hernandez, A., Kelly, G. A., Li, X., Onogi, K.,
3 Saarinen, S., Sokka, N., Allan, R. P., Andersson, E., Arpe, K., Balmaseda, M. A.,
4 Beljaars, A. C. M., Van de Berg, L., Bidlot, J., Bormann, N., Caires, S., Chevallier,
5 F., Dethof, A., Dragosavac, M., Fisher, M., Fuentes, M., Hagemann, S., Hólm, E.,
6 Hoskins, B. J., Isaksen, L., Janssen, P. A. E. M., Jenne, R., McNally, A. P., Mahfouf,
7 J. -F., Morcrette, J., -J., Rayner, N. A., Saunders, R. W., Simon, P., Sterl, A.,
8 Trenberth, K. E., Untch, A., Vasiljevic, D., Viterbo, P., and Woollen, J.: The ERA-40
9 re-analysis. *Q. J. Roy. Meteor. Soc.*, 131, 2961-3013, 2005.

10 Van de Wal, R. S. W., and Oerlemans, J.: An Energy-Balance Model for the
11 Greenland Ice-Sheet. *Global Planet. Change*, 9, 115-131, 1994.

12 Van den Broeke, M.: Partitioning of melt energy and meltwater fluxes in the ablation
13 zone of the west Greenland ice-sheet. *The Cryosphere*, 2, 179-189, 2008.

14 Van den Broeke, M., Bamber, J., Ettema, J., Rignot, E., Schrama, E., Jan van de Berg,
15 W., van Meijgaard, E., Velicogna, I., and Wouters, B. .: Partitioning Recent
16 Greenland mass Loss. *Science*, 326, 984-986, 2009.

17 Van der Veen, C. J., and Payne, A. J.: Modelling land-ice dynamics. In: *Mass Balance*
18 of the Cryosphere Observations and Modelling of Contemporary and Future Changes,
19 Bamber, J. L., and Payne, A. J. (Eds.), Cambridge University Press, Cambridge UK,
20 169-219, 2004.

21 Velicogna, I.: Increasing rates of ice mass loss from the Greenland and Antarctic ice-
22 sheets revealed by GRACE. *Geophys. Res. Lett.*, 36, L19503,
23 doi:10.1029/2009GL040222, 2009.

24 Vizcaíno, M., Mikolajewicz, U., Gröger, M., Maier-Reimer, E., Schurgers, G., and
25 Winguth, A. M. E.: Long-term ice-sheet-climate interactions under anthropogenic
26 greenhouse forcing simulated with a complex Earth system Model. *Clim. Dynam.*,
27 31,6, doi: 10.1007/s00382-008-0369-7, 2008.

1 Wramneby, A., Smith, B., Zaehle, S., and Sykes, M. T.: Parameter uncertainties in the
2 modelling of vegetation dynamics - Effects on tree community structure and
3 ecosystem functioning in European forest biomes. *Ecol. Model.*, 216, 277-290, 2008.

4 Yang, D. Q.: An improved precipitation climatology for the Arctic Ocean. *Geophys.*
5 *Res. Lett.*, 26, 1625-1628, 1999.

6
7 Zwinger, T., Greve, R., Gagliardini, O., Shiraiwa, T., and Lly, M.: A full Stokes-
8 flow thermo-mechanical model for firn and ice applied to the Gorshkov crater glacier,
9 Kamchatka. *Ann. Glaciol.*, 45, 29-37, 2007.

10

11

12

13

14

15

16

17

18

19

20

21

22

23

24

25

26

27

28

29

30

31

32

33

1 Table 1. List of default parameters and physical constants used in the model. Those
 2 highlighted in bold are varied in the tuning experiments (for a complete set see Rutt et
 3 al. (2009)).

Symbol	Value	Units	Description
ρ_i	910	kg m^{-3}	Density of ice
g	9.81	m s^{-2}	Acceleration due to gravity
a	1.733×10^3	$\text{Pa}^{-3} \text{s}^{-1}$	Material constant for $T^* \geq 263\text{K}$
a	3.613×10^{-13}	$\text{Pa}^{-3} \text{s}^{-1}$	Material constant for $T^* < 263\text{K}$
Q	139×10^3	J mol^{-1}	Activation energy for creep for $T^* \geq 263\text{K}$
Q	60×10^3	J mol^{-1}	Activation energy for creep for $T^* < 263\text{K}$
R	8.314	$\text{J mol}^{-1} \text{K}^{-1}$	Universal gas constant
α_i	8	$\text{mm water d}^{-1} \text{C}^{-1}$	Positive degree day factor of ice
α_s	3	$\text{mm water d}^{-1} \text{C}^{-1}$	Positive degree day factor of snow
L_G	-6.227	$^{\circ}\text{C km}^{-1}$	Atmospheric temperature lapse rate
n	3	-	Flow law exponent
f	3	-	Flow enhancement factor
G	-0.05	W m^{-2}	Uniform Geothermal heat flux

4

5

6

7

8

9

10

11

12

13

14

15

16

1 | Table 2. Summary of sensitivity experiments to changing boundary condition/forcing
2 | individually from that used in the EISMINT-3 exercise to more recent datasets.

Bedrock & ice thickness	Precipitation	Temperature
Bamber et al. (2001)	EISMINT-3	EISMINT-3
EISMINT-3	Era-40	EISMINT-3
EISMINT-3	EISMINT-3	Hanna et al. (2005)
Bamber et al. (2001)	Era-40	Hanna et al. (2005)

3
4
5
6
7
8
9
10
11
12
13
14
15
16
17
18
19
20
21
22
23
24
25
26
27

1 Table 3. Summary of the relative difference between updated boundary
2 condition/forcing and the EISMINT-3 datasets. Positive values correspond to an
3 increase and negative values a decrease in ice volume/ice surface extent. Note when
4 all boundary conditions/forcings are updated the relative change almost equal the sum
5 of the individual changes.

	Update bedrock	Update precip	Update temp	Update all
	& ice elv.			
<i>Ice volume (%)</i>	+13.65	-0.04	+1.64	+16.92
<i>Ice surface extent (%)</i>	+11.49	+2.07	+0.43	+14.08

6

7

8

9

10

11

12

13

14

15

16

17

18

19

20

21

22

23

24

25

26

27

28

29

1 | Table 43. List of five parameters varied according to the ranges determined from the
 2 literature. α_s , α_i , G and f are similar to those used in Ritz et al. (1997).

Parameter	Minimum value	Maximum value
Positive degree day factor for snow, α_s (mm $d^{-1}^{\circ}C^{-1}$)	3	5
Positive degree day factor for ice, α_i (mm $d^{-1}^{\circ}C^{-1}$)	8	20
Enhancement flow factor, f	1	5
Geothermal heat flux, G ($\times 10^{-3}$ mW m $^{-2}$)	-61	-38
Near surface lapse rate, L_G ($^{\circ}C km^{-1}$)	-4.0	-8.2

3
 4
 5
 6
 7
 8
 9
 10
 11
 12
 13
 14
 15
 16
 17
 18
 19
 20
 21
 22
 23
 24
 25
 26
 27

1 Table 5. Tuned parameter values for the five optimal experiments chosen according to
 2 diagnostic skill score.

Diagnostic	f	L_G ($^{\circ}\text{C km}^{-1}$)	G ($\times 10^{-3} \text{ mW m}^{-2}$)	α_s ($\text{mm d}^{-1} \text{C}^{-1}$)	α_i ($\text{mm d}^{-1} \text{C}^{-1}$)
<i>Ice vol. & NRMSE</i>					
<i>ice thk</i>					
10	4.5838	-4.2047	-52.630	3.7243	19.878
233	4.8585	-4.0754	-46.667	4.2425	16.344
<i>Surf. area</i>					
99	1.2838	-4.5334	-41.758	4.7844	18.710
<i>Surf. area & NRMSE ice thk</i>					
165	3.1036	-4.2456	-47.709	4.5763	19.455
<i>Max. alt.</i>					
67	2.6165	-8.1157	-53.421	3.9951	13.502
240	2.5551	-6.0820	-59.070	3.6258	10.221

3

4

5

6

7

8

9

10

11

12

13

14

15

16

17

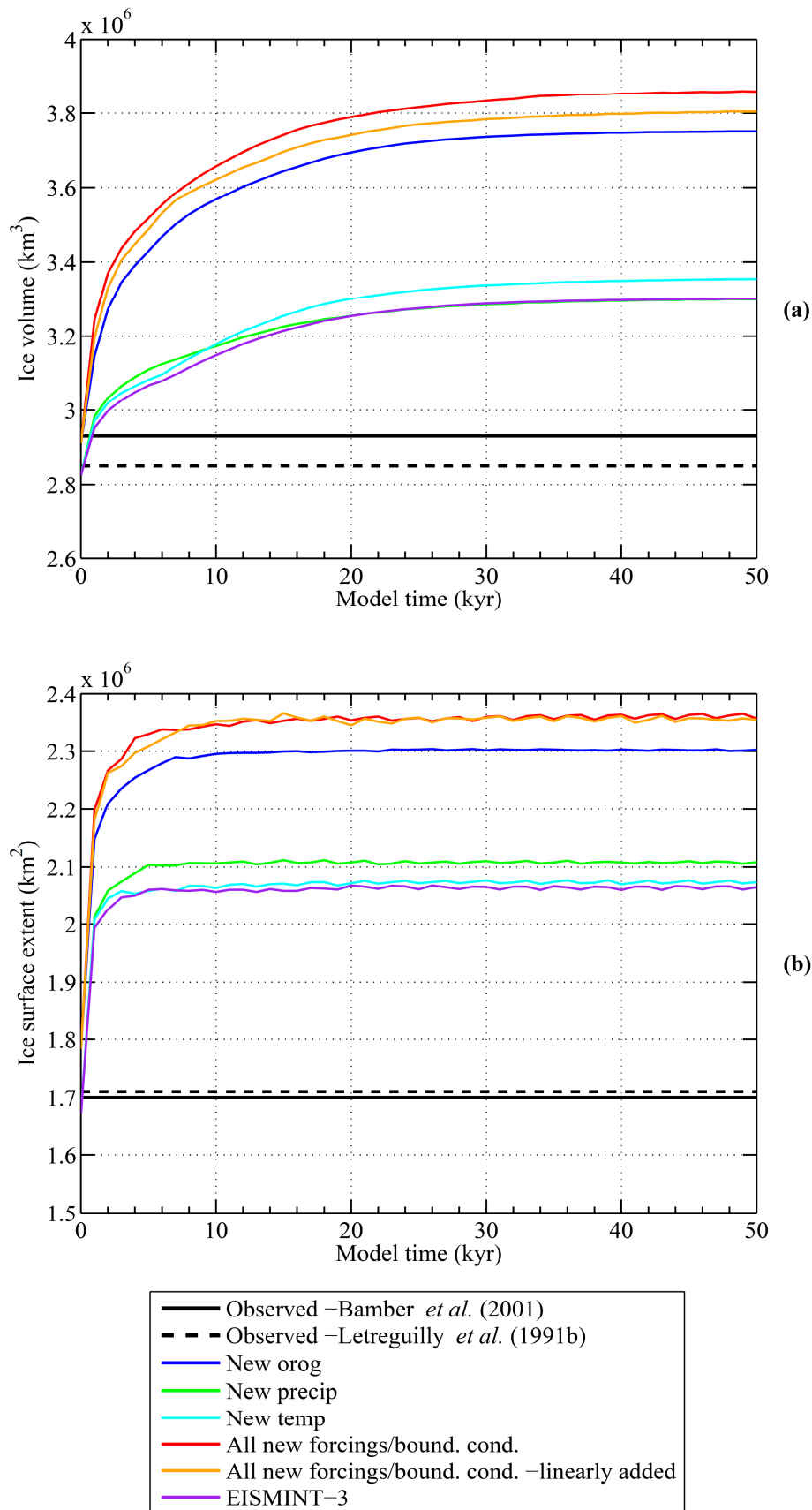
18

19

20

21

22



1 | Figure 1. Evolution of the modelled ice-sheet a) volume and b) ice surface extent for
2 | each of the different boundary conditions and forcings changed one at a time relative
3 |

1 to EISMINT-3, when they are all varied together, and when they are linearly
2 combined. The EISMINT-3 experiment is also shown for comparison, and
3 observations derived from Bamber et al. (2001) and Letreguilly et al. (1991) are also
4 shown for comparison.

5

6

7

8

9

10

11

12

13

14

15

16

17

18

19

20

21

22

23

24

25

26

27

28

29

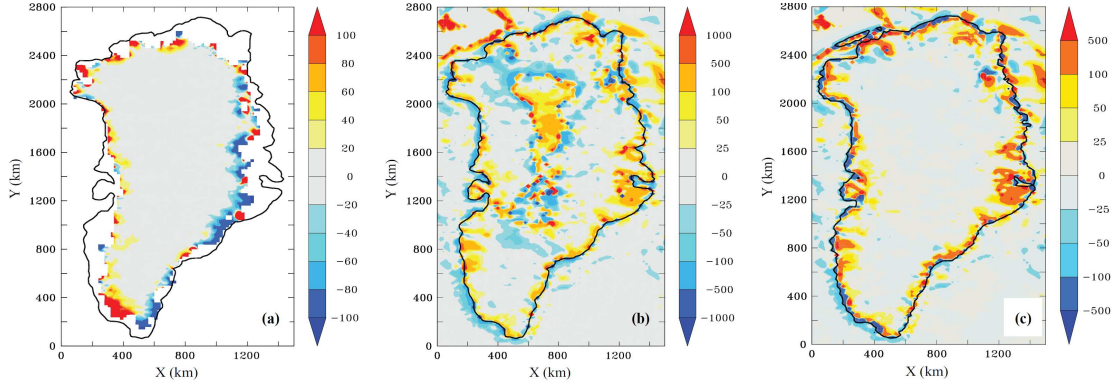
30

31

32

33

34



1 Figure 2. (a) The ratio of the difference of ice thickness of Bamber dataset and ice
 2 thickness of Letreguilly dataset ($z_{\text{bamber}} - z_{\text{letreguilly}} / z_{\text{letreguilly}}$) expressed as a percentage.
 3 The regions of largest relative difference occur around the margins with good
 4 agreement between the datasets in the ice-sheet interior. (b) The ratio of the
 5 difference in initial bedrock topography of Bamber dataset and the topography of
 6 Letreguilly expressed as a percentage. Again the largest differences occur around the
 7 margins of Greenland and also in the central region where the bedrock is below sea
 8 level (c) The ratio of the difference in relaxed bedrock topography after the removal
 9 of ice and isostatic equilibrium has been reached expressed as a percentage. The
 10 resultant orography shows the relative difference around the margins of up to 500%,
 11 with Bamber orography significantly higher.
 12
 13
 14
 15
 16
 17
 18
 19
 20
 21
 22
 23
 24
 25
 26
 27

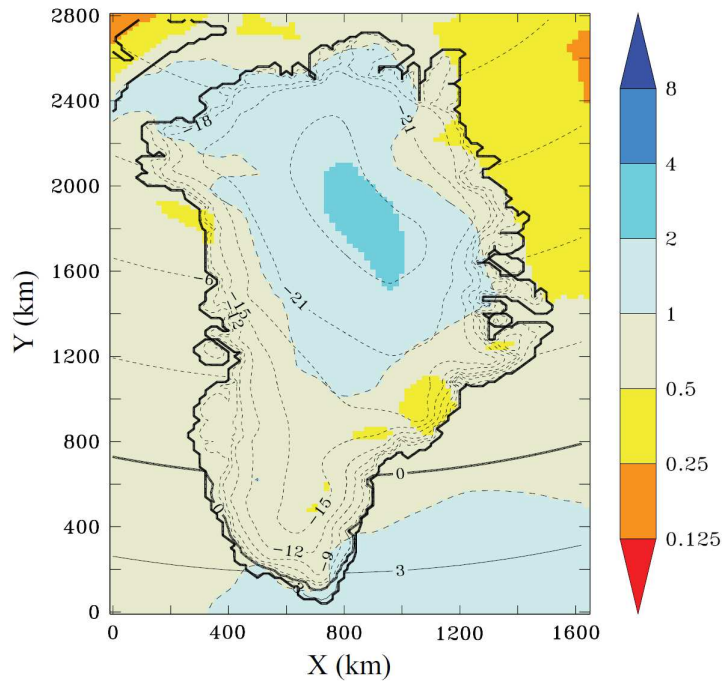


Figure 32. Change in precipitation (in m/yr) over Greenland between EISMINT-3 (Ohmura and Reeh, 1991) and ERA-40 re-analysis (Uppala et al. 2005) expressed as a ratio of EISMINT-3:ERA-40. Annual surface temperature (in $^{\circ}\text{C}$) contours also shown.

1

2

3

4

5

6

7

8

9

10

11

12

13

14

15

16

17

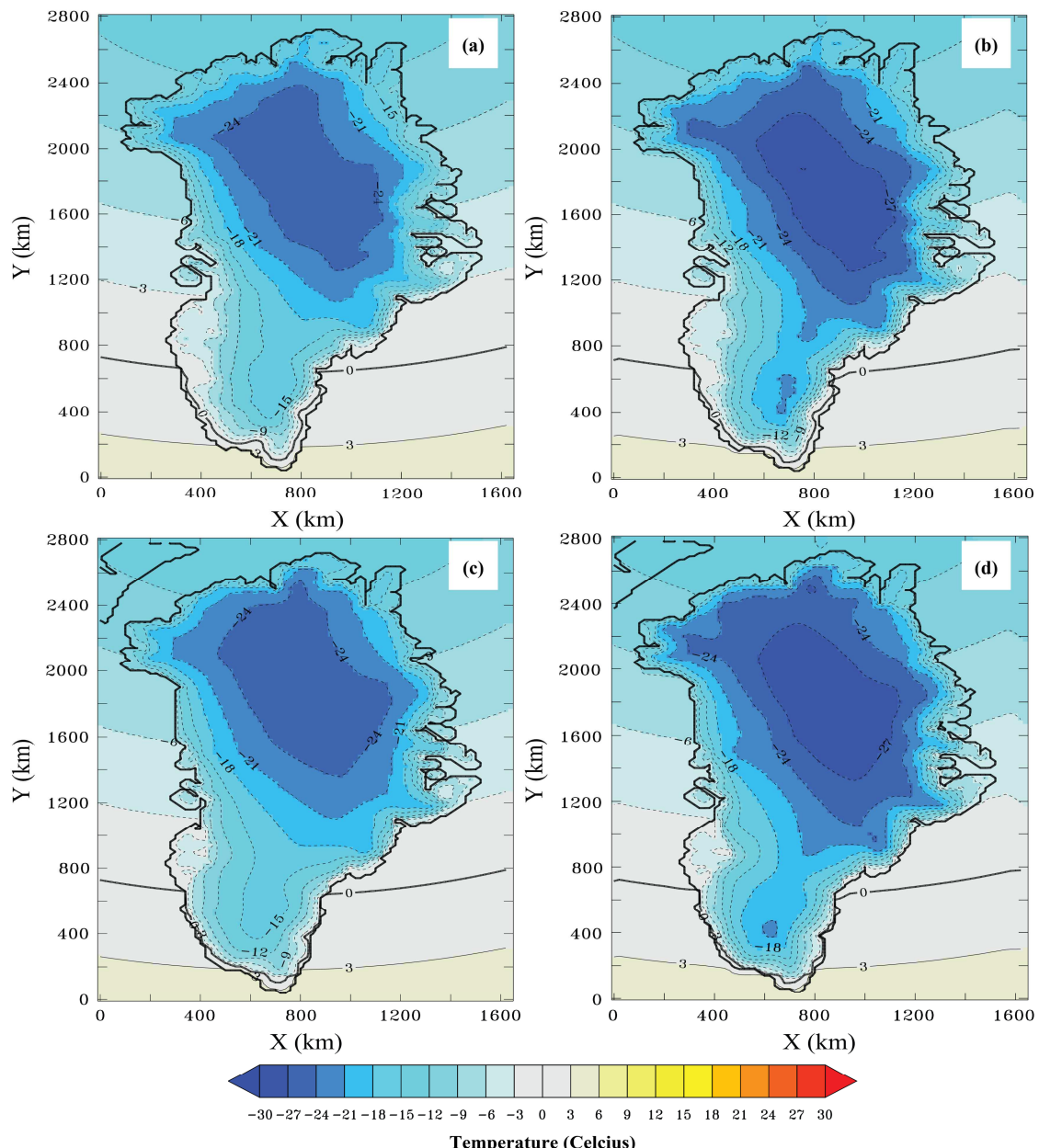
18

19

20

21

22



1

2 | Figure 43. Sensitivity to different temperature forcings for the GrIS. The near surface
 3 | air-temperature (in °C) over Greenland for a) after 1 year of model time forced with
 4 | EISMINT-3 temperatures, b) after 1 year of model time forced with Hanna modified
 5 | temperatures, c) after 50,000 years of model time forced with EISMINT-3
 6 | temperatures and d) after 50,000 years of model time forced with Hanna modified
 7 | temperatures.

8

9

10

11

12

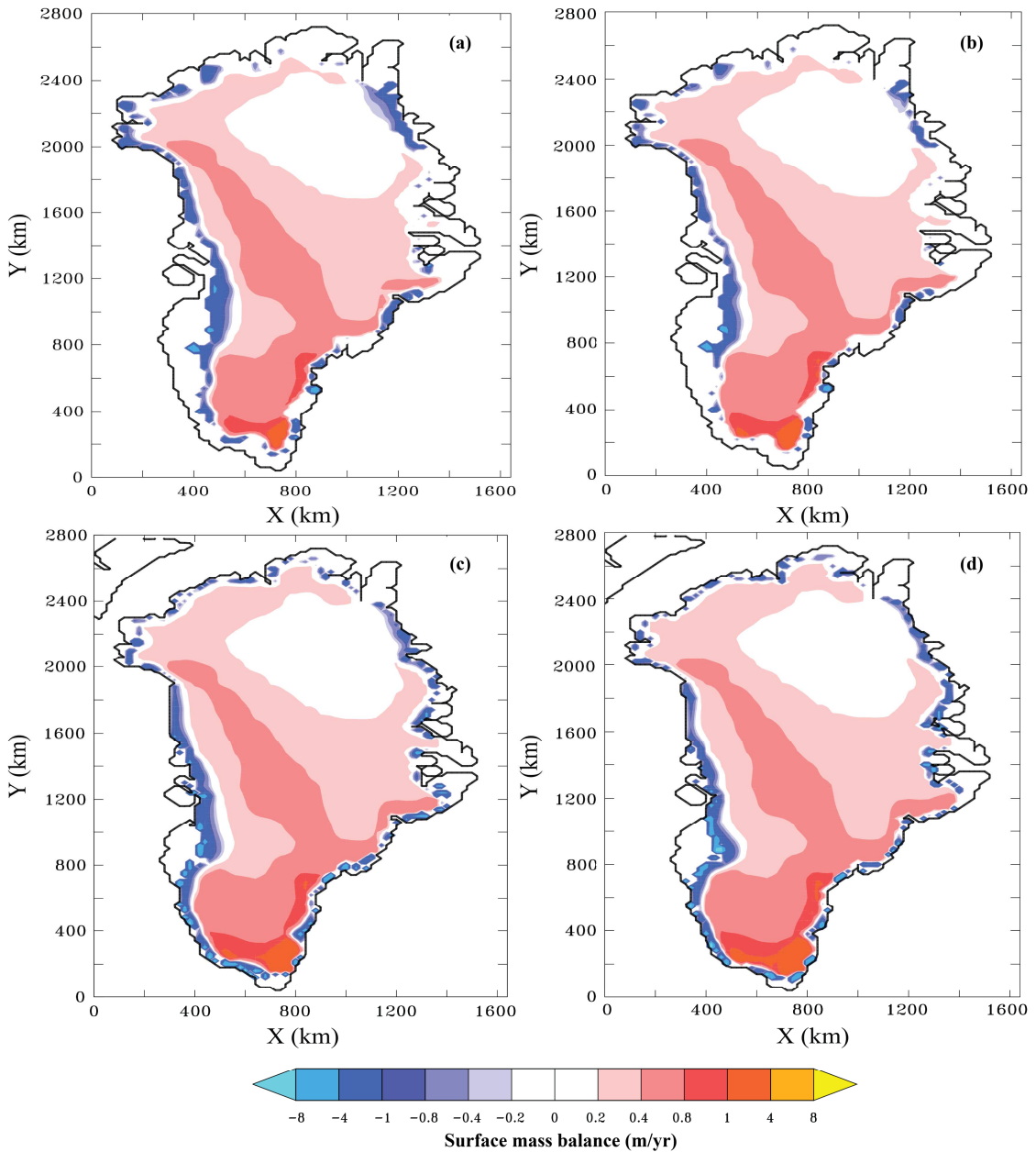
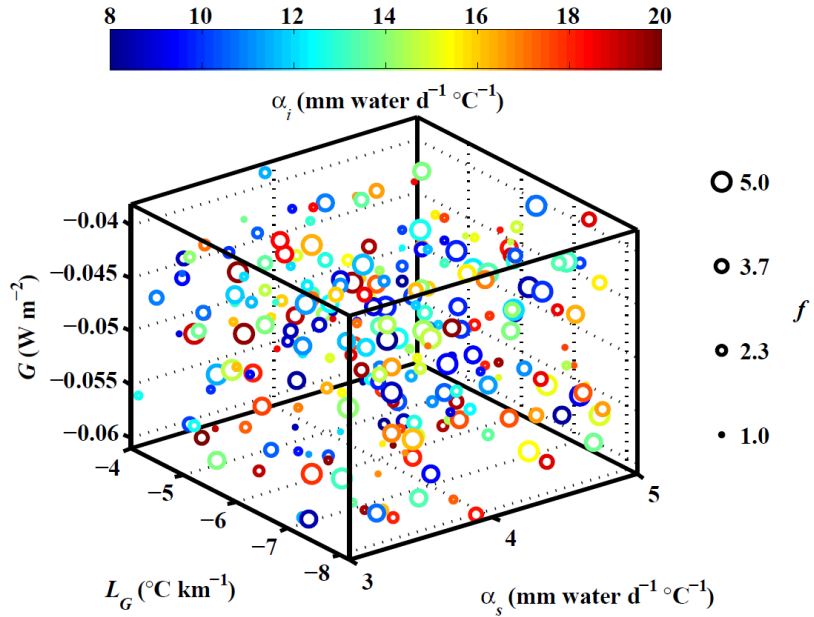


Figure 54. Sensitivity to different temperature forcings for the GrIS. The net surface mass balance (in m/yr) over Greenland for a) after 1 year of model time forced with EISMINT-3 temperatures b) after 1 year of model time forced with Hanna modified temperatures, c) after 50,000 years of model time forced with EISMINT-3 temperatures and d) after 50,000 years of model time forced with Hanna modified temperatures. Note the non-linearity of the scale.



1 Figure 6. Distribution of 250 experiments produced by Latin-Hypercube Sampling. In
 2 three dimensions geothermal heat flux (G), PDD factor for snow (α_s) and atmospheric
 3 vertical lapse rate (L_G) are shown. In addition, for each experiment the PDD factor
 4 for ice (α_i) is shown in terms of the colour-scale and the enhancement flow factor (f)
 5 in terms of the size of circle.

6

7

8

9

10

11

12

13

14

15

16

17

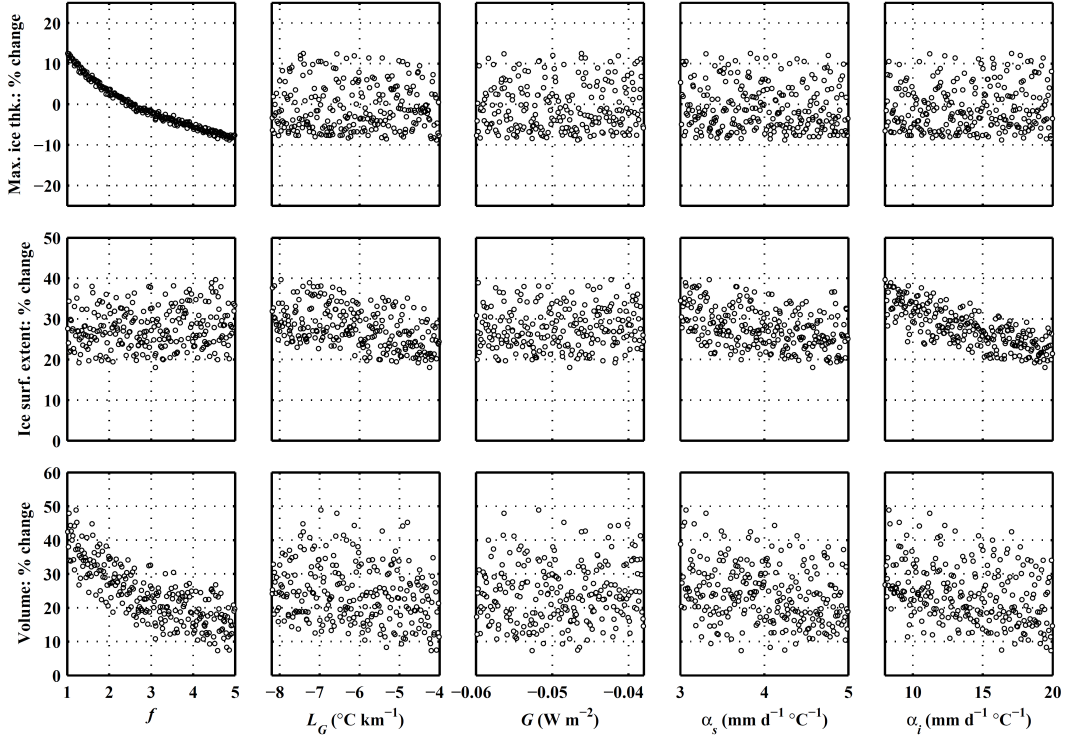
18

19

20

21

22



1 Figure 7. Sensitivity of three diagnostics describing the response of ice-sheet
 2 geometry (volume, ice surface extent and maximum ice thickness) to different values
 3 of the enhancement flow factor (f), the atmospheric lapse rate (L_G), the geothermal
 4 heat flux (G) and the ice (α_i) and snow (α_s) PDD factors for the calculation of
 5 ablation. All values correspond to the end of the simulation at 50,000 years where
 6 equilibrium is reached.

7

8

9

10

11

12

13

14

15

16

17

18

19

20

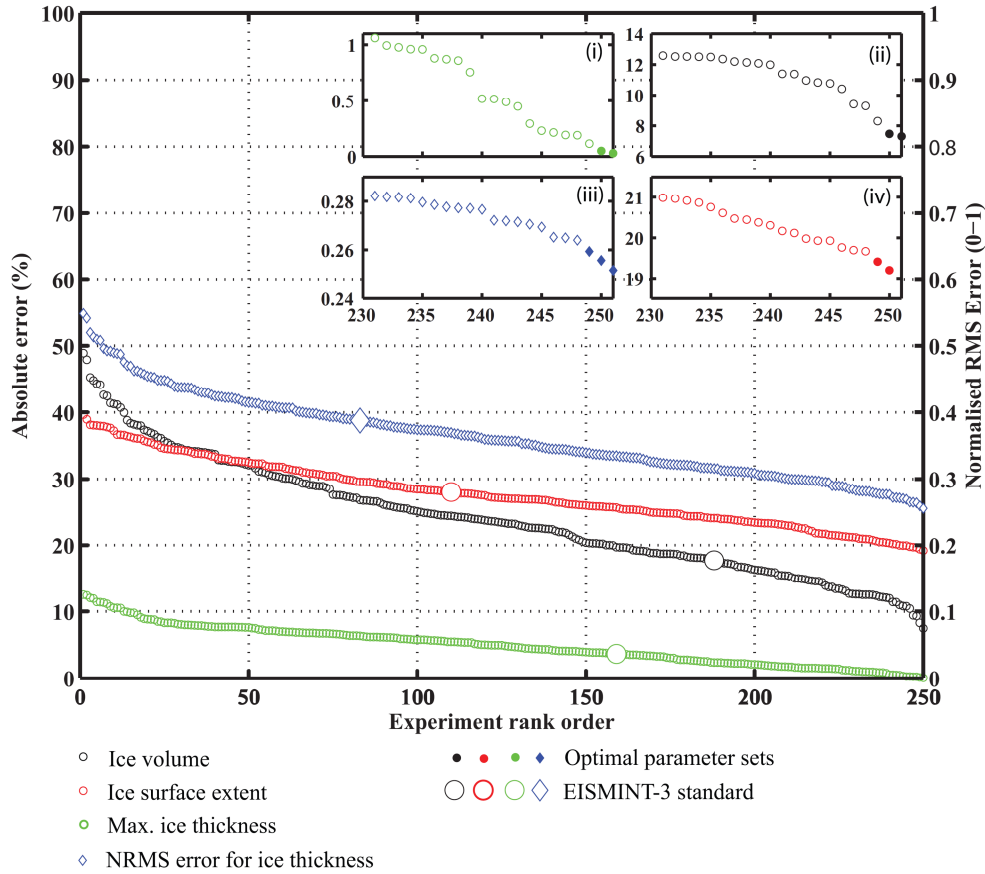
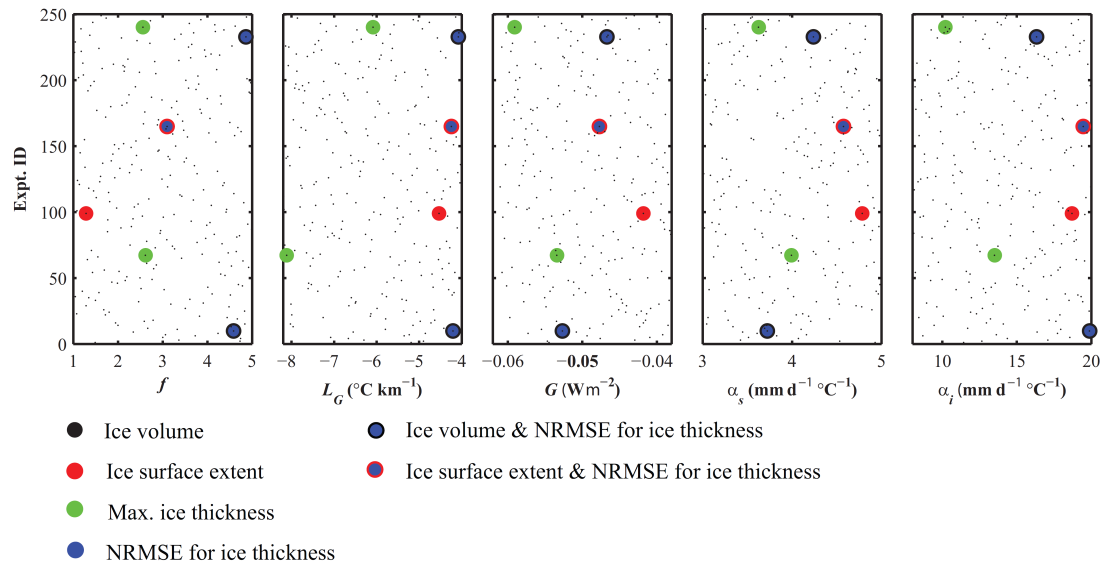


Figure 8. Ranking of LHSsensitivity experiments for ice volume, ice surface extent and maximum ice thickness each diagnostic skill score according to absolute error (left) and NRMSE for ice thickness (right). The experiments rank from least agreement (1) to the closest agreement with observation (251). Observations here are taken from Bamber et al. (2001) on the 20-km resolution grid. The left hand axis represents the absolute error skill score which is used for the diagnostics represented by circles where 0 is perfect agreement. These are as follows: volume, ice surface extent and maximum ice thickness. The right hand vertical axis represents the NRMSE error for ice thickness with 0 being perfect agreement. The larger symbols represent where the rank position of the standard EISMINT-3 experiment. The inset graphss show the optimal experiments zoomed in for ranking from from 230 to 251 for (i) maximum ice thickness, (ii) ice volume, (iii) NRMSE for ice thickness and (iv) ice surface extent. The y-scale for each insetaxes are isalso zoomed in on independently for each diagnostic in order to see the change in gradient more clearly. Filled circles/diamonds represent the optimal parameter sets for reproducing the modern day GrIS.



1 | Figure 9. The distribution of each parameter for the ~~eight-six~~ experiments selected
 2 | according to ranking of the different diagnostics: volume, ice surface extent and
 3 | maximum ice thickness. Experiment ID number is shown on the y-axis (from 1-250)
 4 | with its corresponding parameter values on the x-axis. ~~The experiments highlighted~~
 5 | ~~with a black box are the ones selected according to the spread for that particular~~
 6 | ~~parameter~~. The small black dots represent all 250 experiments to show the parameter
 7 | space covered.

8

9

10

11

12

13

14

15

16

17

18

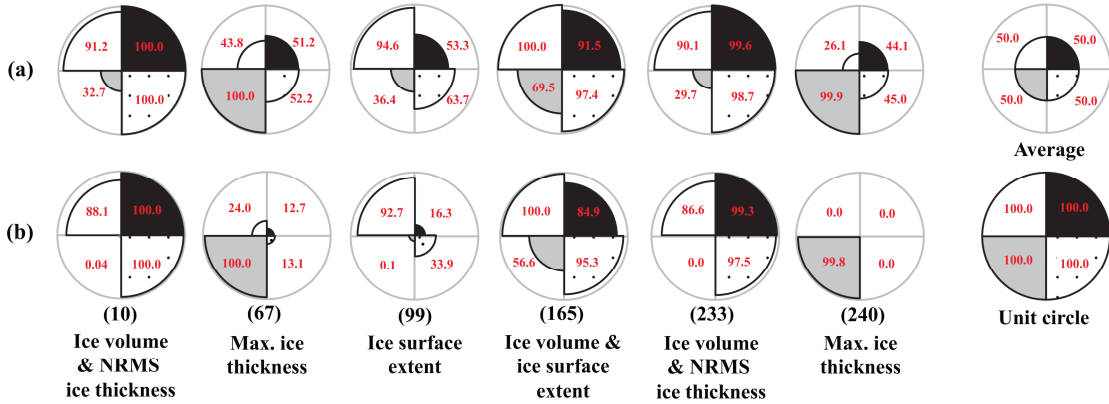
19

20

21

22

23



1  Figure 10. Normalised star plots showing the relative measure of skill for each
2 diagnostic. The best skill score corresponds to a radius of 100 % as shown by the unit
3 circle. Relative measure of skill for a) the ~~six-five~~ selected experiments compared
4 with all 250 LHS ~~sensitivity~~ experiments and b) the final ~~six-five~~ chosen experiments
5 compared with each other. The numbers below each experiment correspond to the
6 experiment identification number relating to the original 250 ~~tuning-LHS~~ experiments.
7
8
9
10
11
12
13
14
15
16
17
18
19
20
21
22
23
24
25
26

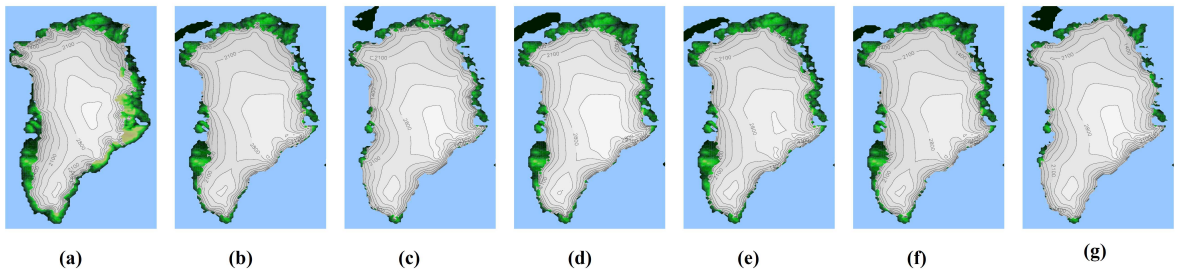
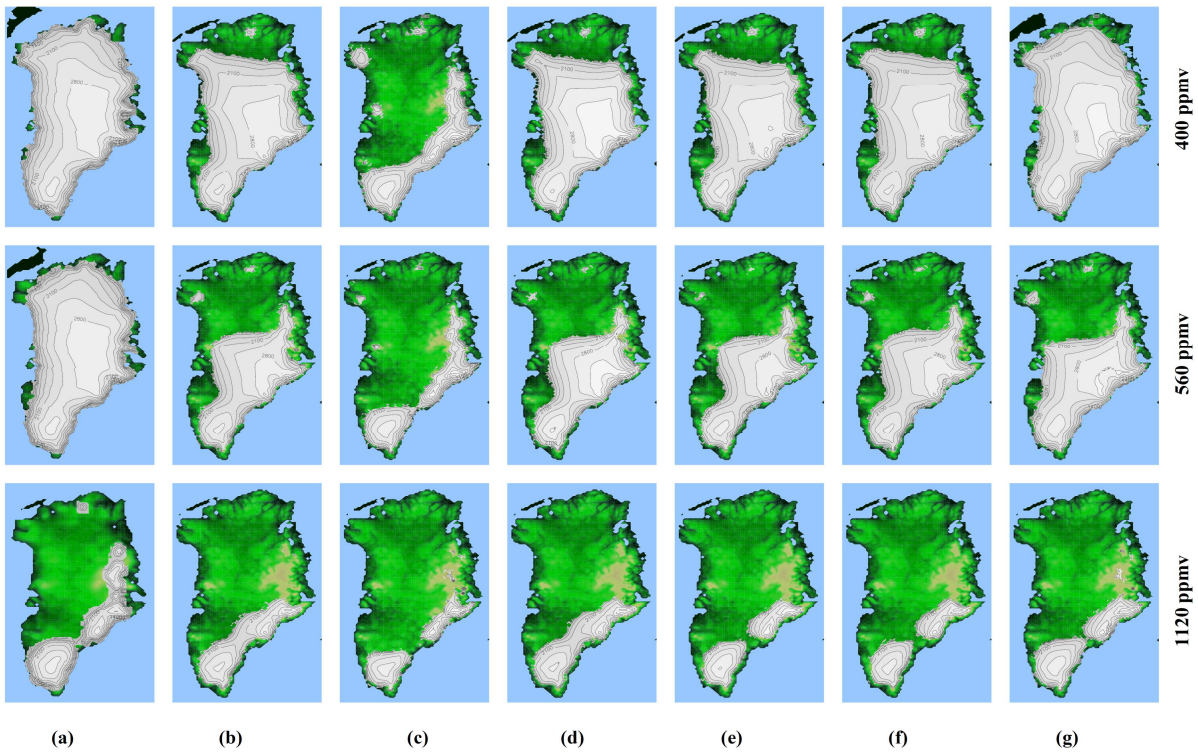


Figure 11. Ice-sheet configurations for a) observed present day GrIS (from Bamber et al., 2001) and b) to f) configurations for the ~~six~~^{five} selected experiments shown in Table 4-5 and Figure 10 (experiment ID numbers [10](#), [67](#), [99](#), [165](#), [233](#) and [240](#) ~~63~~, [233](#), [78](#), [181](#), [230](#) respectively).

1
2
3
4
5
6
7
8
9
10
11
12
13
14
15
16
17
18
19
20
21
22
23
24
25
26
27
28
29



1

2 | Figure 12. Ice-sheet [configurations-geometry](#) for future warming scenarios (400
 3 | ppmv, 560 ppmv and 1120 ppmv CO₂) for a) standard EISMINT-3 setup as shown in
 4 | Lunt et al. (2009) and b) to f) the selected parameter sets from tuning (experiments
 5 | [ID-numbers 10, 67, 99, 165, 233 and 240 respectively](#)
 6 | [63, 233, 78, 181, 230 respectively](#)). See Table 54 for the tuned parameter [values-sets](#) corresponding to these
 7 | particular experiments.

8

9

10

11

12

13

14

15

16

17

18

19

20